JASA ARTICLE

Contributions of gravity waves in the ocean to *T*-phase excitation by earthquakes[a)]

Oleg A. Godin[b)]
Department of Physics, Naval Postgraduate School, 833 Dyer Road, Monterey, California 93943-5216, USA

ABSTRACT:
The generation of *T* waves in a deep ocean by an earthquake in its epicentral region is often observed, but the mechanism of the excitation of the acoustic waves travelling horizontally with the speed of sound remains controversial. Here, the hypothesis is investigated that the abyssal *T* waves are generated by the scattering of ballistic sound waves by surface and internal gravity waves in the ocean. Volume and surface scattering are studied theoretically in the small perturbation approximation. In the 3–50 Hz typical frequency range of the observed *T* waves, the linear internal waves are found to lack the necessary horizontal spatial scales to meet the Bragg scattering condition and contribute appreciably to the *T*-wave excitation. In contrast, the ocean surface roughness has the necessary spatial scales at typical sea states and wind speeds. The efficiency of the acoustic normal modes' excitation at surface scattering of the ballistic body waves by wind seas and sea swell is quantified and found to be comparable to that of the established mechanism of the *T*-wave generation at downslope conversion at the seamounts. The surface scattering mechanism is consistent with key observational features of the abyssal *T* waves, including their ubiquity, low-frequency cutoff, presence on seafloor sensors, and weak dependence on the earthquake focus depth. https://doi.org/10.1121/10.0007283

(Received 8 July 2021; revised 26 October 2021; accepted 28 October 2021; published online 23 November 2021)
[Editor: Nicholas P. Chotiros] Pages: 3999–4017

I. INTRODUCTION

The *T*-, or tertiary, phase of an underwater earthquake is composed of low-frequency acoustics waves, which propagate to long ranges in the underwater waveguide at speeds close to the sound speed in water and arrive later than *P*-, or primary, and *S*-, or secondary phases, which are due to the compressional (*P*) and shear (*S*) body waves in the seabed, and later than the seismo-acoustic interface waves.[1–4] The *T* waves weakly attenuate with the range, travel over very large distances, and are observed throughout the World Ocean. They are the most common earthquake sounds in the ocean and make strong but transient contributions to the ambient sound field.[5,6] A comprehensive review of *T*-wave research up to the mid-2000s can be found in Refs. 2, 3, 7, and 8.

In addition to the hydrophones at various depths in the water column,[9–13] *T* waves are routinely observed by receivers on the seafloor in deep water,[14–16] which indicates, in agreement with the full-wave numerical modeling,[8,12,17–19] that *T* waves are not confined in the Sound Fixing and Ranging (SOFAR) channel. Because the wave speed and absorption in water are, respectively, smaller and much smaller than in the Earth's crust, *T* waves prove to be the most sensitive and rather accurate means to detect, characterize, and localize the marine teleseismic events, including weak intraplate events.[9,20–23] In addition, *T* waves carry information about the ocean. It was proposed to use measurements of the temporal variability of the *T*-wave travel times to characterize the internal tides and associated ocean mixing[24] and, more recently, for ocean acoustic thermometry.[25,26]

Numerous observations show that the conversion of seismic energy into guided acoustic waves in the oceanic waveguide occurs in the vicinity of the earthquake epicenter and at prominent bathymetric features, which may be located hundreds of kilometers away from the epicenter.[3,9,13,20,27–31] The *T*-wave amplitudes remain significant for intermediate-depth earthquakes[9,32] and are insensitive to the water depth.[2] *T* waves from deep-focus earthquakes with hypocenter depths of hundreds of kilometers have been also observed.[3,14] The conversion mechanism and especially *T*-wave excitation in the immediate vicinity of the epicenter are not well understood.[2,8,22] The excitation of acoustic normal modes at large-scale bathymetric features can be explained in terms of the downslope conversion and diffraction of the *P* and *S* body waves and/or seismo-acoustic interface waves by horizontally inhomogeneous bathymetry.[8,19,33–36] The ubiquitous "abyssal" *T* waves,[9,32,33,37] which are generated near the epicenter of earthquakes under flat abyssal planes, cannot be attributed to any of these generation mechanisms. Unlike the trapping of acoustic energy in the SOFAR channel by the downslope conversion of steeply propagating sound, the generation of abyssal *T* waves does not lend itself to a ray interpretation. It had been realized early on[9,32,37] that a wave scattering mechanism was required to explain the abyssal *T*-wave observations. Johnson *et al*. discussed the scattering at the ocean surface and seafloor and volume scattering of sound in the ocean

[a)]Portions of this work were presented in "On the possible role of gravity waves in the ocean in T-phase excitation by earthquakes," 178th Meeting of the Acoustical Society of America, San Diego, CA, December 2019.
[b)]Electronic mail: oagodin@nps.edu, ORCID: 0000-0003-4599-2149.

among the conceivable generation mechanisms and favored scattering by the ocean surface.[9,32,37] However, their crude estimates of the generation efficiency were not encouraging. Keenan and Merriam[38] proposed sound scattering from keels on the undersurface of the ice cover as the mechanism of generation of abyssal T waves in the Arctic. The idea that sound scattering at the ocean surface could be an important mechanism of T-phase generation has been recently revisited by Bottero[8] using full-wave, two-dimensional (2-D) numerical modeling in a scenario with strong, discrete scatterers located on the ocean surface.

Following Fox *et al.*[20] and De Groot-Hedlin and Orcutt,[39,40] it is often implied in the current literature[3,6,22] that abyssal T waves are generated as a result of wave scattering by the seafloor roughness, specifically due to coupling between the seismo-acoustic normal modes, which are directly excited by the seismic source, and the normal modes comprising the T-phase.[41,42] By modeling the scattered waves as the field due to the uncorrelated virtual sound sources distributed along the seafloor, De Groot-Hedlin and Orcutt[39,40] and Yang and Forsyth[22] have successfully reproduced the shapes of the envelopes of the observed T-phase waveforms. However, detailed information about the seafloor roughness spectra is rarely if ever available around the epicenter of abyssal earthquakes with the granularity and at the spatial scales necessary for the T-phase modeling. To our knowledge, the amplitude of the resulting T waves has never been related to the actual seafloor roughness data or models in a quantitative manner and is shown to be sufficient to explain the observed abyssal T waves.

Here, we examine an alternative hypothesis that the sound waves coming at steep angles directly from the earthquake focus (ballistic body waves) are coupled to the normal modes of the underwater acoustic waveguide by dynamic processes in the water column and on the ocean surface. Specifically, we investigate the generation of abyssal T waves at the scattering of ballistic sound waves by the ocean surface roughness, which is the result of the surface gravity waves, and volume inhomogeneities of the water column, which are caused by the internal gravity waves. We view the ocean surface and volume scattering as either complementary to the seafloor scattering or possibly an alternative mechanism of the generation of abyssal T waves. Unlike the seafloor roughness data in the open ocean, extensive information on the statistics of the wind waves and sea swell[43–45] and internal gravity wave spectra[46,47] is available, which allows one to reach definitive conclusions regarding the significance of these generation mechanisms.

T waves are a seismo-acoustic phenomenon with representative wave frequencies being very high on the seismic scale and low for underwater sound. Typically, T waves are observed in the 1–100 Hz band.[2,3] The lower frequencies dominate the signals from stronger and deeper earthquakes, whereas the highest frequencies are generated by the weakest detected seismic events. Abyssal T waves exhibit higher frequencies than the T waves generated at the down-slope conversion.[3,32] Therefore, this paper will focus on the 3–50 Hz frequency band that contains most of the abyssal T-wave energy. The observations indicate the existence of a low-frequency cutoff in the T-phase spectra; see, e.g., Refs. 13, 32, 48, and Ref. 8, p. 59. The low-frequency cutoff will be related to the T-phase generation process in this paper.

Mathematically, we describe the excitation of abyssal T waves as scattering from the continuous spectrum into the discrete spectrum of the seismo-acoustic field. The continuous spectrum is represented here by the body waves, which are generated by an earthquake and reach the water column with a modest transmission loss at typical T-phase frequencies below about 40–50 Hz. This process is reciprocal of the scattering of the normal modes propagating in the oceanic waveguide by the rough ocean surface and/or volume inhomogeneities caused by the internal gravity waves (scattering from the discrete into the continuous spectrum of the acoustic field). In that problem, a part of the scattered energy is radiated into the seabed and carried away from the waveguide, leading to the well-known contribution to attenuation of the normal modes.[49–52]

The remainder of the paper is organized as follows. A theory of the excitation of acoustic normal modes at the scattering of a low-frequency body wave by a rough ocean surface and random volume inhomogeneities is developed in Sec. II for underwater waveguides with either a fluid or solid bottom. The efficiency of the T-phase excitation by ballistic body waves is related to the spectral properties of the roughness and volume inhomogeneities. The theory is applied in Sec. III to surface scattering by wind seas with the Pierson-Moskovitz spectrum and wavetrains of the sea swell to characterize the frequency spectra, directionality, and energy of the resulting T waves and the dependence of the T-phase properties on the earthquake focus depth. Simple, order-of-magnitude estimates of the T-phase energy are obtained in Sec. IV A and employed to argue that the surface scattering of ballistic body waves in the vicinity of the earthquake epicenter is a significant T-phase generation mechanism with a strength comparable to that of a seamount at a moderate distance from the epicenter. Section IV B discusses the possible extensions of the theory to quantify other plausible mechanisms of the generation of T waves and related waves in the atmosphere. Section V summarizes our findings.

II. *T*-PHASE GENERATION BY SURFACE AND VOLUME SCATTERING

A. Scattering of low-frequency sound by the rough ocean surface

Consider a horizontally stratified ocean of depth H. Introduce Cartesian coordinates x, y, and z with the vertical coordinate z increasing downward. The mean position of the ocean surface is the horizontal plane $z = 0$, and the seafloor is located at $z = H$ (Fig. 1). The epicenter of an earthquake, which generates T waves, is located in the vicinity of the origin $x = 0$, $y = 0$ of the horizontal coordinates. In addition to the Cartesian coordinates, we will also use a cylindrical

https://doi.org/10.1121/10.0007283

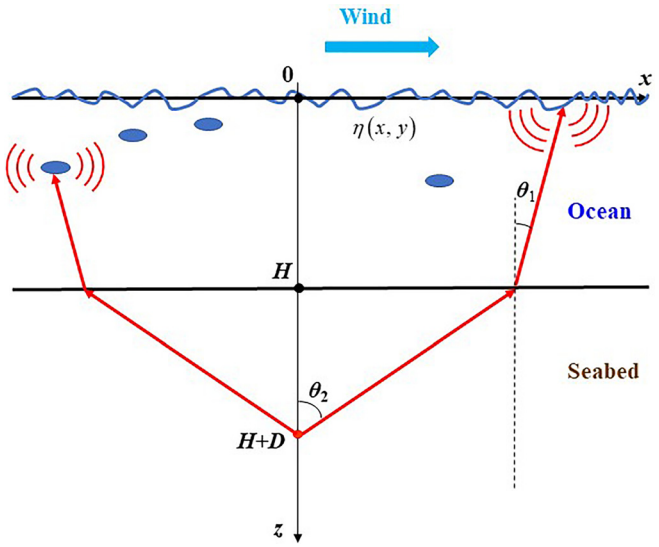

FIG. 1. (Color online) The geometry of the problem. The ballistic waves from the earthquake focus scatter at the rough ocean surface and volume inhomogeneities in the water column, which act as secondary sound sources and generate guided waves in the oceanic waveguide. The volume inhomogeneities are symbolically represented by ovals in the figure. The ocean surface roughness is described by the surface elevation η, which varies with the horizontal coordinates x and y. The earthquake focus is located at $x = y = 0$ at the depth $z = H + D$ under the seafloor $z = H$.

coordinate system $\{r,\varphi,z\}$ with the same z axis. When averaged over the perturbations resulting from the internal gravity waves, the sound speed c in the ocean and water density ρ, as well as the density and compressional and shear wave speeds in the seabed, are functions of z. We disregard the seafloor roughness and effects of the horizontal inhomogeneities of the water column and seabed when considering the wave scattering by the ocean surface roughness.

The wave heights on the ocean surface are small compared to the acoustic wavelengths at the T-phase frequencies (longer than 30 m for frequencies below 50 Hz). With a possible exception for some breaking waves, the slopes of the ocean surface are small compared to unity. The sound scattering by such surfaces can be described by the small perturbation method.[53,54] Consider the scattering of monochromatic acoustic waves of frequency ω by a stationary (frozen) rough surface. We will use the complex notation for monochromatic wave fields, where the time dependence $\exp(-i\omega t)$ of the acoustic pressure and other quantities is assumed and suppressed. In the first approximation of the small perturbation method, the acoustic pressure p_{sc} in the wave scattered by a rough pressure-release surface is

$$p_{sc}(\mathbf{R}) = -\int \left[\frac{\partial p_0}{\partial z_1}\frac{\partial G(\mathbf{R};\mathbf{r}_1,z_1)}{\partial z_1}\right]_{z_1=0} \eta(\mathbf{r}_1)\frac{d\mathbf{r}_1}{\rho}. \tag{1}$$

Here, integration is over the mean surface $z = 0$; $\mathbf{r}_1$ is a 2-D horizontal vector, $\mathbf{R}$ is a three-dimensional (3-D) position vector; p_0 is the acoustic pressure in the monochromatic wave in the absence of surface roughness, i.e., in the "unperturbed" waveguide with the pressure-release boundary $z = 0$. The acoustic pressure in the full acoustic field in water equals $p_{sc} + p_0$; p_0 contains the incident wave and the wave reflected from the flat (horizontal) ocean surface. The surface elevation $\eta(\mathbf{r})$ is the vertical deviation of the rough surface from the mean plane $z = 0$. Mathematically, the rough surface is given by the equation $z = \eta(\mathbf{r})$. Note that $p_{sc} \to 0$ in the limit $\eta \to 0$ of the vanishing roughness. In Eq. (1), $G(\mathbf{R};\mathbf{R}_1)$ is the acoustic Green's function in the ocean with the flat upper boundary $z = 0$. The Green's function has the meaning of the acoustic pressure at point $\mathbf{R}$ due to a point sound source of the volume velocity located at $\mathbf{R}_1$. In the water column, the Green's function satisfies the equation,[55]

$$\frac{\partial}{\partial \mathbf{R}}\left[\frac{1}{\rho}\frac{\partial}{\partial \mathbf{R}}G(\mathbf{R};\mathbf{R}_1)\right] + \frac{\omega^2}{\rho c^2}G(\mathbf{R};\mathbf{R}_1) = -\delta(\mathbf{R}-\mathbf{R}_1), \tag{2}$$

as well as the appropriate boundary conditions on the ocean surface and seafloor. Here, $\delta(\mathbf{R})$ is the Dirac delta function. The approximate solution [Eq. (1)] for the scattered wave describes the single scattering from the rough surface but accounts for all of the multiple reflections in the ocean with the horizontal upper boundary.[53–55]

The physical meaning of Eq. (1) is that in the first approximation of the small perturbation method, the waves scattered from the rough ocean surface are described as the waves generated by a known, distributed sound source in the ocean with the flat upper boundary. Indeed, the acoustic pressure in the field generated by the monochromatic sound sources in an inhomogeneous fluid satisfies the reduced wave equation,[55]

$$\nabla\cdot\left(\frac{\nabla p}{\rho}\right) + \frac{\omega^2}{\rho c^2}p = i\omega A + \nabla\cdot\left(\frac{\mathbf{F}}{\rho}\right), \tag{3}$$

where $\mathbf{F}$ and A stand for the volume densities of the external force and volume velocity (i.e., the volume injection rate), respectively. In terms of the acoustic Green's function G of the medium, the solution of the reduced wave equation is given by[55]

$$p(\mathbf{R}) = \int\left[\frac{\mathbf{F}(\mathbf{R}_1)}{\rho(\mathbf{R}_1)}\cdot\frac{\partial G(\mathbf{R};\mathbf{R}_1)}{\partial \mathbf{R}_1} - i\omega A(\mathbf{R}_1)G(\mathbf{R};\mathbf{R}_1)\right]d\mathbf{R}_1, \tag{4}$$

where the integration is over the entire volume occupied by the sources. The comparison of Eqs. (1) and (4) shows that in the first approximation of the small perturbation method, the scattered wave coincides with the field that would be generated in the medium with the horizontal upper boundary by external forces with a density of

$$\mathbf{F}(\mathbf{r}_1,z_1) = \left(0,\quad 0,\quad -\eta(\mathbf{r}_1)\frac{\partial p_{\text{in}}}{\partial z_1}\delta(z_1)\right). \tag{5}$$

Equation (5) describes an effective vertical external force applied on the horizontal ocean surface. The effective sound

source depends on the incident wave and roughness of the actual ocean surface.

One can also reach the same conclusion that the scattered wave in an inhomogeneous medium is equivalent to the sound field generated by the effective sound source [Eq. (5)] on the horizontal boundary by comparing the boundary condition[53,54] $p_{sc}(\mathbf{r}_1, z = +0) = -\eta(\mathbf{r}_1)(\partial p_{in}/\partial z_1)_{z_1=0}$ for the scattered wave in the first approximation of the small perturbation method with the discontinuity (jump)[55] $p(\mathbf{r}_1, z = +0) - p(\mathbf{r}_1, z = 0) = p(\mathbf{r}_1, z = +0) = F_{0z}(\mathbf{r}_1)$ of the acoustic pressure, which, according to Eq. (3), is caused by the distribution of the external vertical forces with the volume density $F_{0z}\delta(z)$ just below a pressure-release boundary $z = 0$. Here, $z = +0$ denotes the points situated below the boundary $z = 0$ infinitesimally close to it.

B. Excitation of normal modes at the surface scattering

In a horizontally stratified oceanic waveguide with a fluid seabed, the acoustic Green's function is given by the sum of normal modes,[55,56]

$$G(\mathbf{R};\mathbf{R}_1) = \frac{i}{4}\sum_n f_n(z)f_n(z_1)H_0^{(1)}(\xi_n|\mathbf{r}-\mathbf{r}_1|) = \sum_n f_n(z)f_n(z_1)\frac{\exp(i\xi_n|\mathbf{r}-\mathbf{r}_1| + i\pi/4)}{\sqrt{8\pi\xi_n|\mathbf{r}-\mathbf{r}_1|}} \times \left[1 + O\left(\frac{1}{\xi_n|\mathbf{r}-\mathbf{r}_1|}\right)\right], \quad (6)$$

plus a contribution of the continuous spectrum. The latter is usually negligible at long-range propagation. Here, $H_0^{(1)}(\bullet)$ is a Hankel function of the first kind of order zero, ξ_n and $f_n(z)$ are the propagation constant and shape function of the nth normal mode, $n = 1,2,\ldots$, respectively. The shape functions are normalized by the condition

$$\int_0^\infty \frac{dz}{\rho(z)} f_n^2(z) = 1. \quad (7)$$

The shape function $f_n(z)$ gives the vertical dependence of the acoustic pressure in the nth normal mode. When the horizontal separation of the points $\mathbf{R} = (\mathbf{r},z)$ and $\mathbf{R}_1 = (\mathbf{r}_1,z_1)$ is large compared to the wavelength, the Hankel function can be replaced by the dominant term of its asymptotic expansion,[57] leading to the rightmost side in Eq. (6). With the points $\mathbf{R}$ and $\mathbf{R}_1$ located in water, Eq. (6) remains valid in the waveguide with the stratified solid seabed,[58] but instead of Eq. (7), the normalization condition of the normal mode shape functions in the fluid-solid waveguide takes the form

$$\int_0^H \rho^{-1} f_n^2 dz + \frac{\omega}{\xi_n}\int_H^{+\infty} (\tau_{xz}v_z - \tau_{xx}v_x)\rho dz = 1, \quad (8)$$

where H is the water depths, τ_{xx} and τ_{xz} are the components of the stress tensor, and v_x and v_z are the components of the particle velocity $\mathbf{v} = (v_x,0,v_z)$ in the seabed in the nth normal mode with the dependence $\exp(i\xi_n x)$ of its field on the horizontal coordinates.[58] The shape functions $f_n(z)$ are real-valued in the absence of dissipation. The physical meaning of the normalization equation (8) is that the modes with the same amplitude carry the same power flux; the acoustic power flux J_n in a single propagating normal mode with $p(\mathbf{r},z) = af_n(z)H_0^{(1)}(\xi_n r)$, where a is a constant, equals $J_n = 2|a^2|/\omega$.[55,56,58]

Substitution of the Green's function [Eq. (6)] into Eq. (1) for the scattered wave and changing the order of the summation and integration gives

$$p_{sc}(\mathbf{r},z) = \sum_n \frac{f_n(z)\exp(-3i\pi/4)}{\sqrt{8\pi\xi_n}\rho(0)}\frac{\partial f_n}{\partial z}\bigg|_{z=0} Q_n(\mathbf{r}), \quad (9)$$

$$Q_n(\mathbf{r}) = \int d\mathbf{r}_1 \frac{\exp(i\xi_n|\mathbf{r}-\mathbf{r}_1|)}{\sqrt{|\mathbf{r}-\mathbf{r}_1|}}\eta(\mathbf{r}_1)\frac{\partial p_0}{\partial z_1}(\mathbf{r}_1, z_1 = 0), \quad (10)$$

provided that $\xi_n\,|\mathbf{r}-\mathbf{r}_1\,| \gg 1$. Equation (9) represents the scattered wave in the waveguide as a sum of the normal modes, where $f_n(z)$ is the dependence of the acoustic pressure on the depth in the nth normal mode. In the summand, the factor in front of Q_n is controlled by the waveguide's properties and the receiver depth. The dependence on the horizontal coordinates of the receiver, the incident wave, and the properties of the rough surface is described by the factor Q_n [Eq. (10)]. When discussing the scattered wave, we will refer to Q_n as the mode amplitude for brevity.

Equations (9) and (10) show that each normal-mode component of p_{sc} is a result of the interference of the contributions generated by the scattering at different points on the rough surface. A more intuitive derivation of the normal-mode representation [Eqs. (9) and (10)] of the scattered wave is obtained using the concept of the effective sources of the scattered wave. The surface density of the effective vertical force on the flat surface of a horizontally stratified oceanic waveguide is given by Eq. (5). A point source of the vertical force with $\mathbf{F}(\mathbf{r}_1,z_1) = (0,\ 0,\ F_0\delta(\mathbf{r}_1)\delta(z_1))$ generates the acoustic field[56]

$$p(\mathbf{R}) = \frac{iF_0}{4\rho(z_1)}\sum_n f_n(z)\frac{\partial f_n(z_1)}{\partial z_1}H_0^{(1)}(\xi_n|\mathbf{r}-\mathbf{r}_1|) \quad (11)$$

in the waveguide. Here, as in Eq. (6) for the Green's function, we disregard the continuous spectrum of the field. Adding the contributions [Eq. (11)] of the elementary effective sources located at different points on the boundary, i.e., by calculating the convolution of the field of a unit vertical force with the source density Eq. (5), again leads to Eqs. (9) and (10).

Equation (10) can be further simplified in the far field of the distributed effective source of the scattered wave. However, the far field assumption proves to be too restrictive to be useful in the T-phase excitation problem. For orientation, with the effective source dimensions of $L_T = O(10\,\text{km})$ and sound frequency $f \sim 20\,\text{Hz}$ the far field condition $r \gg \xi_n L_T^2$ requires the range r from the epicenter to be more than 10 Mm. Here, we will obtain the more relevant and widely applicable results by taking into account

https://doi.org/10.1121/10.0007283

that the correlation scale of the ocean surface roughness is much smaller than L_T.

As discussed in Sec. III C, the extensive areas on the ocean surface can contribute to T-phase generation, and we need to allow for variations of the surface roughness statistics within these areas. Let the ocean surface elevation $\eta(\mathbf{r})$ have zero mean and be a locally stationary random function,[53] then $\langle\eta(\mathbf{r})\rangle = 0$ and

$$\langle\eta(\mathbf{r}_1)\eta(\mathbf{r}_2)\rangle = C\left(\mathbf{r}_1 - \mathbf{r}_2; \frac{\mathbf{r}_1 + \mathbf{r}_2}{2}\right). \tag{12}$$

Here and below, the angular brackets $\langle\cdot\rangle$ denote the statistical average; C has the meaning of the correlation function of the surface elevations. The characteristic spatial scales l and L of the variation of the correlation function with respect to the difference $\mathbf{r}_1 - \mathbf{r}_2$ and centroid $0.5(\mathbf{r}_1 + \mathbf{r}_2)$ coordinates satisfy the condition $l \ll L$. In the particular case of the wide-sense stationary random elevations, $L \to \infty$ and the correlation function C depends only on $\mathbf{r}_1 - \mathbf{r}_2$. In terms of the correlation function, the root mean square (rms) surface elevation σ_η and the roughness spectrum are given by the equation $\sigma_\eta = \langle\eta^2(\mathbf{r})\rangle^{1/2} = \sqrt{C(0;\mathbf{r})}$ and

$$S_\eta(\mathbf{q};\mathbf{r}) = (2\pi)^{-2}\int C(\mathbf{r}_1;\mathbf{r})\exp(-i\mathbf{q}\cdot\mathbf{r}_1)d\mathbf{r}_1. \tag{13}$$

The spectrum and rms elevation of the surface roughness gradually vary with the position $\mathbf{r}$.

At the reflection from the random rough surface, mode amplitudes [Eq. (10)] are also random, and $\langle Q_n(\mathbf{r})\rangle = 0$. For the mode amplitude variance from Eqs. (10) and (12), we find

$$\begin{aligned}\langle|Q_n^2(\mathbf{r})|\rangle = \int d\mathbf{r}_1 d\mathbf{r}_2 \frac{\exp[i\xi_n(|\mathbf{r}-\mathbf{r}_1| - |\mathbf{r}-\mathbf{r}_2|)]}{\sqrt{|\mathbf{r}-\mathbf{r}_1||\mathbf{r}-\mathbf{r}_2|}} \\ \times C\left(\mathbf{r}_1 - \mathbf{r}_2; \frac{\mathbf{r}_1+\mathbf{r}_2}{2}\right)\frac{\partial p_0(\mathbf{r}_1,0)}{\partial z} \\ \times\left(\frac{\partial p_0(\mathbf{r}_2,0)}{\partial z}\right)^*.\end{aligned} \tag{14}$$

Here and below, the asterisk "*" denotes complex conjugation. The main contribution to the integral is from such $\mathbf{r}_1$ and $\mathbf{r}_2$ that $|\mathbf{r}_1 - \mathbf{r}_2|$ is on the order of or smaller than the roughness correlation scale l. When the horizontal separation r from the epicenter is large compared to the size L_T of the effective source of the scattered wave and $r \gg \xi_n l^2$, one can approximate the product $|\mathbf{r} - \mathbf{r}_1||\mathbf{r} - \mathbf{r}_2|$ with r^2 in the integrand in Eq. (14) and retain in the exponent only linear terms of the developments,

$$\begin{aligned}&\left|\mathbf{r} - \frac{\mathbf{r}_1+\mathbf{r}_2}{2} \pm \frac{\mathbf{r}_1-\mathbf{r}_2}{2}\right| \\ &= \left|\mathbf{r} - \frac{\mathbf{r}_1+\mathbf{r}_2}{2}\right| \pm \left|\mathbf{r} - \frac{\mathbf{r}_1+\mathbf{r}_2}{2}\right|^{-1} \\ &\times\left(\mathbf{r} - \frac{\mathbf{r}_1+\mathbf{r}_2}{2}\right)\cdot\frac{\mathbf{r}_1-\mathbf{r}_2}{2} + O\left(\frac{|\mathbf{r}_1-\mathbf{r}_2|^2}{|2\mathbf{r}-\mathbf{r}_1-\mathbf{r}_2|}\right),\end{aligned} \tag{15}$$

of $|\mathbf{r} - \mathbf{r}_j|$, $j = 1,2$, in powers of $|\mathbf{r}_1 - \mathbf{r}_2|$. We also assume that the unperturbed field p_0 can be represented as

$$p_0(\mathbf{r},z) = P(\mathbf{r},z)\exp[i\mathbf{q}_{\text{in}}(\mathbf{r})\cdot\mathbf{r}] \tag{16}$$

in the vicinity of the ocean surface in water. Here, the complex amplitude P and the local horizontal wave vector $\mathbf{q}_{\text{in}}$ are gradually varying functions of $\mathbf{r}$, which are little changed over the distances $O(l)$.

Changing the integration variables in Eq. (14) from $\mathbf{r}_1$ and $\mathbf{r}_2$ to the difference and centroid position vectors, $\mathbf{r}_1 - \mathbf{r}_2$ and $\mathbf{r}_3 = 0.5(\mathbf{r}_1 + \mathbf{r}_2)$, and using Eqs. (13), (15), and (16), we obtain a compact expression for the mode amplitude variance,

$$\begin{aligned}&\langle|Q_n^2(\mathbf{r})|\rangle = \frac{4\pi^2}{r}\int d\mathbf{r}_3\left|\frac{\partial P(\mathbf{r}_3,0)}{\partial z}\right|^2 S_\eta(\xi_n\mathbf{e} - \mathbf{q}_{\text{in}};\mathbf{r}_3), \\ &\mathbf{e} = \frac{\mathbf{r}-\mathbf{r}_3}{|\mathbf{r}-\mathbf{r}_3|}.\end{aligned} \tag{17}$$

Here, $\mathbf{e}$ has the meaning of the unit horizontal vector from an elementary scatterer to the observation point, and $\xi_n\mathbf{e}$ is the horizontal wave vector of the nth mode propagating from $\mathbf{r}_3$ to $\mathbf{r}$. For the distant observation points that we consider, it is close to the unit horizontal vector from the epicenter to the observation point: $\mathbf{e} = r^{-1}\mathbf{r} + O(L_T/r)$. Inspection shows that Eq. (17) is consistent with the more general result, Eq. (9) in Ref. 59, for the cross-correlation function of the surface reverberation in the oceanic waveguide.

Integration in Eq. (17) is over the entire horizontal plane $z = 0$. The ocean surface area, which significantly contributes to the normal mode excitation, is controlled by the decrease in the amplitude of the unperturbed field p_0 with the horizontal separation from the epicenter and is affected by the spatial distribution of the surface roughness. The integrand is proportional to the average power scattered into the nth mode in the vicinity of the point $(\mathbf{r}_3,0)$ on the ocean surface. The contributions of different points into the average mode's power are added incoherently, according to Eq. (17). The first argument, $\xi_n\mathbf{e} - \mathbf{q}_{\text{in}}$, of the roughness spectrum, S_η, in the integrand equals the change of the horizontal wave vector of sound at the scattering and corresponds to Bragg's scattering, which is expected in the first approximation of the small perturbation method.[53,54] We will use Eq. (17) in Sec. III to investigate the effects on the T-phase generation of the wind speed, sea swell parameters, and depth of the earthquake focus.

The acoustic power flux in the T waves can be calculated by integrating the power flux density over the cylindrical surface $r = \text{const.} > L_T$, $0 < z < \infty$. At distances r from the epicenter, which are large compared to the diameter L_T of the region, where the T waves are excited, $\nabla Q_n \approx i\xi_n r^{-1}Q_n\mathbf{r}$, according to Eq. (10). Using the normalization condition (8), for the power flux J_n in the nth mode, we find

$$J_n = \frac{r}{16\pi\omega}\left(\frac{1}{\rho}\frac{\partial f_n}{\partial z}\right)^2_{z=0}\int_0^{2\pi}|Q_n^2(r\cos\varphi, r\sin\varphi)|d\varphi \tag{18}$$

from Eq. (9). The total power flux is given by the sum of the contributions J_n [Eq. (18)] of all of the propagating normal modes. For a random rough surface with the spectrum S_η, Eqs. (17) and (18) give

$$\langle J_n\rangle = \frac{\pi}{4\omega}\left(\frac{1}{\rho}\frac{\partial f_n}{\partial z}\right)^2_{z=0}\int_0^{2\pi}\left[\int d\mathbf{r}_3\left|\frac{\partial P(\mathbf{r}_3,0)}{\partial z}\right|^2 \times S_\eta(\xi_n\mathbf{e}-\mathbf{q}_{\rm in};\mathbf{r}_3)\right]d\varphi, \tag{19}$$

where $\mathbf{e} = (\cos\varphi,\sin\varphi,0)$. As expected, the power flux is independent of r as long as the effect of the absorption on the propagating normal mode is negligible over ranges on the order of r.

C. Excitation of normal modes at the volume scattering by internal gravity waves

Consider internal gravity waves propagating in an otherwise horizontally stratified, stationary ocean. The internal wave-induced currents, $\mathbf{u}$, and variations of the sound speed, δc, and density, $\delta\rho$, from their unperturbed (background) values, $c(z)$ and $\rho(z)$, are horizontally inhomogeneous. The currents are slow and the environmental perturbations are weak in the following sense: $|\delta c| + u \ll c$, $\delta\rho \ll \rho$. Neglecting terms of the second order in the small ratio u/c, the monochromatic acoustic waves satisfy the following wave equation[55,60] in the horizontally inhomogeneous ocean with slow currents:

$$\nabla\cdot\left(\frac{\nabla p}{\rho_0}\right)+\frac{\omega^2}{\rho_0 c_0^2}p+\frac{2i\omega}{\rho_0 c_0^2}\mathbf{u}\cdot\nabla p-\frac{2i}{\omega}\nabla\cdot\left(\frac{1}{\rho_0}\sum_{j=1}^{3}\frac{\partial p}{\partial x_j}\frac{\partial \mathbf{u}}{\partial x_j}\right)=0. \tag{20}$$

Here, $\rho_0 = \rho + \delta\rho$, $c_0 = c + \delta c$, and $(x_1,x_2,x_3) = (x,y,z)$ are the Cartesian coordinates. The acoustic pressure $p = p_0 + p_{\rm sc}$ consists of the acoustic pressure p_0 in the horizontally stratified ocean and the perturbation (scattered wave) $p_{\rm sc}$. In the water column, p_0 satisfies Eq. (20) with $\mathbf{u} = \mathbf{0}$ and ρ_0 and c_0 replaced with ρ and c, respectively.

The scattered wave vanishes when the environmental perturbations $\mathbf{u}$, δc, and $\delta\rho$ vanish. Retaining only the terms of the first order in the acoustic and environmental perturbations, from Eq. (20), we find

$$\nabla\cdot\left(\frac{\nabla p_{\rm sc}}{\rho}\right)+\frac{\omega^2}{\rho c^2}p_{\rm sc} = i\omega A_{\rm sc}+\nabla\cdot\left(\frac{\mathbf{F}_{\rm sc}}{\rho}\right), \tag{21}$$

where

$$A_{\rm sc} = \frac{-i\omega p_0}{\rho c^2}\left(\frac{\delta\rho}{\rho}+\frac{2\delta c}{c}\right)-\frac{2}{\rho c^2}\mathbf{u}\cdot\nabla p_0,$$
$$\mathbf{F}_{\rm sc} = \frac{\delta\rho}{\rho}\nabla p_0+\frac{2i}{\omega}\sum_{j=1}^{3}\frac{\partial p_0}{\partial x_j}\frac{\partial \mathbf{u}}{\partial x_j}. \tag{22}$$

The above assumptions correspond to the calculation of the scattered wave in the single-scattering or (first) Born approximation. The comparison of Eqs. (3) and (21) shows that in the Born approximation, the scattered wave can be viewed as the wave generated in the horizontally stratified ocean by distributed virtual sources with volume densities $A_{\rm sc}$ and $\mathbf{F}_{\rm sc}$ [Eq. (22)], respectively, of the volume velocity and external force. Using Eq. (4) for the field of distributed sources and Eq. (6) for the Green's function, we find the scattered wave in the following form:

$$p_{\rm sc}(\mathbf{r},z) = \sum_n \frac{f_n(z)\exp(-i\pi/4)}{\sqrt{8\pi\xi_n}}V_n(\mathbf{r}), \tag{23}$$

where

$$V_n(\mathbf{r}) = \int d\mathbf{r}_1\frac{\exp(i\xi_n|\mathbf{r}-\mathbf{r}_1|)}{\sqrt{|\mathbf{r}-\mathbf{r}_1|}} \times\int\frac{dz_1}{\rho}\left[\left(\omega\rho A_{\rm sc}+\xi_n\frac{\mathbf{r}-\mathbf{r}_1}{|\mathbf{r}-\mathbf{r}_1|}\cdot\mathbf{F}_{\rm sc}\right)f_n + i\frac{\partial f_n}{\partial z_1}(\mathbf{F}_{\rm sc})_z\right], \tag{24}$$

and $(\mathbf{F}_{\rm sc})_z$ stands for the vertical component of the vector $\mathbf{F}_{\rm sc}$, defined in Eq. (22). Equation (23) represents the scattered wave as a sum of the normal modes with V_n describing the dependence of the nth mode amplitude on the horizontal coordinates.

In small-amplitude or linear internal waves, the sound speed and density perturbations are proportional to the vertical displacement ζ of the fluid particles resulting from the internal wave: $\delta c = \alpha_1(z)c\zeta$, $\delta\rho = \alpha_2(z)\rho\zeta$.[46] The vertical velocity u_3 of the fluid particles is given by the time derivative of ζ, and the horizontal components of the velocity are related to ζ by the incompressibility condition $\nabla\cdot\mathbf{u} = 0$.[46] In a random field of linear internal waves, let the vertical displacement ζ have a zero mean and be a random function, which is locally stationary in the horizontal plane. Then the correlation function of the vertical displacements is related to the spatial spectrum S_ζ of internal waves as follows:

$$\langle\zeta(\mathbf{r}_1,z_1)\zeta(\mathbf{r}_2,z_2)\rangle = \int S_\zeta\left(\mathbf{q};z_1,z_2;\frac{\mathbf{r}_1+\mathbf{r}_2}{2}\right)e^{i\mathbf{q}\cdot(\mathbf{r}_1-\mathbf{r}_2)}d\mathbf{q}. \tag{25}$$

Under these assumptions, the densities of the effective sources of the scattered sound wave are also zero-mean random functions, which are locally stationary in the horizontal plane. Using Eq. (22), the spectra of the random sources can be related to the spectrum of the vertical displacement of the fluid particles; importantly, the source spectra have the same spatial scales as those for S_ζ.

At the scattering by random internal waves, the mode amplitudes V_n are random and have zero mean. The calculation of the variance of the mode amplitude and, particularly, the reduction of a double integral over the horizontal coordinate to a single integral, is similar to the calculation of $\langle|Q_n^2|\rangle$ in Sec. II B. From Eqs. (16), (22), (24), and (25), we find that

https://doi.org/10.1121/10.0007283

$$\langle |V_m^2(\mathbf{r})| \rangle = \frac{4\pi^2}{r} \int d\mathbf{r}_3 dz_1 dz_2 \Phi(\mathbf{r}_3, z_1) \Phi(\mathbf{r}_3, z_2)^* \times S_\zeta(\xi_m \mathbf{e} - \mathbf{q}_{\text{in}}; z_1, z_2; \mathbf{r}_3),$$
$$\Phi(\mathbf{r}, z) = \left[\alpha_2 \xi_m \mathbf{e} \cdot \mathbf{q}_{\text{in}} - k^2(2\alpha_1 + \alpha_2)\right] \frac{f_m P}{\rho} + \frac{\alpha_2}{\rho} \frac{\partial P}{\partial z} \frac{\partial f_m}{\partial z}. \quad (26)$$

Here, the unit horizontal vector **e** is the same as that in Eq. (17). For brevity, the contributions of the internal wave-induced currents into the sound scattering are not included in Eq. (26). Equations (17) and (26), which describe the variances of the mode amplitudes that are proportional to the power flux in the respective normal modes resulting, respectively, from the surface and volume scattering, differ by the additional integration over depths z_1 and z_2 of the volume scatterers in Eq. (26). Note that the spatial spectra S_η and S_ζ of the surface elevation and vertical displacement due to internal waves in Eqs. (17) and (26) have the same vector argument $\xi_n \mathbf{e} - \mathbf{q}_{in}$, which equals the difference of the horizontal wave vectors of the normal mode and the incident wave.

Because of the large values of the compressional and shear wave speeds around the earthquake focus, the earthquake-generated incident waves propagate at steep grazing angles in the water column; see Sec. III C for details. Therefore, $|\xi_n \mathbf{e} - \mathbf{q}_{\text{in}}| \sim \xi_n$. The internal wave spectrum peaks around a 5 km horizontal wavelength, while the minimum and maximum internal wave wavelengths in the ocean are about 0.5 km and 50 km, respectively.[46] In the 3–50 Hz frequency range of the observed T waves, the horizontal wavelength $2\pi/\xi_n$ of the acoustic normal modes ranges from about 30 to 500 m. Hence, the internal wave spectrum in the integrand in Eq. (26) has negligibly small values. The short-wave tail of the internal wave spectrum can possibly contribute to the generation of the lowest-frequency T waves away from the earthquake epicenter. In other words, the internal wave field lacks the relatively short horizontal scales (<500 m) that are required for the Bragg scattering of the earthquake-generated body waves into normal modes of the underwater waveguide. As discussed below, the ocean surface roughness spectrum is rich in the spatial scales required for the Bragg scattering into normal modes and, therefore, efficiently contributes to the T-phase generation.

III. CONTRIBUTIONS OF WIND SEAS AND SEA SWELL INTO THE *T*-PHASE GENERATION

A. *T*-phase excitation due to wind seas

The dependence of the ocean surface roughness on the wind speed and fetch have been studied extensively, which allows for a reliable prediction of the T waves generation at the scattering by the sea surface roughness. Here, we use a simple Pierson-Moskovitz model[43,44] of the fully developed wind seas to investigate the dependence of the amplitudes of the normal mode components of the scattered acoustic wave on its frequency, wind speed, and direction of propagation of the incident wave.

The Pierson-Moskovitz spectrum[43,44] of the random surface elevation η is given by the following equations:

$$S_\eta(\mathbf{q}; \mathbf{r}) = W(q) D_W(q, \psi), \quad \int_{-\pi}^{\pi} D_W(q, \psi) d\psi = 1, \quad (27)$$

$$W(q) = \frac{0.024}{q^4} \exp\left(-\frac{0.74 g^2}{q^2 U^4}\right). \quad (28)$$

Here, g is the acceleration due to gravity and U is the wind speed measured at a height of 19.5 m above the sea surface. The factor D_W describes the directionality of the surface waves; $\mathbf{q} = q$ (cos ψ,sin ψ,0) is the wave vector of the waves, and the angle ψ indicates the vector **q** direction. The wind speed may gradually change along the ocean surface: $U = U(\mathbf{r})$, and W and D_W in Eqs. (27) and (28) depend on **r** via U. In the wind waves with the Pierson-Moskovitz spectrum, the spectral peak is located at $q_p = 0.70 g U^{-2}$, and the rms surface elevation is $\sigma_\eta = 0.13 U^2/g$. The wave height rapidly increases, and the spectrum peak shifts toward the longer waves when the wind speed increases [Fig. 2(a)]. According to Eq. (28), the spectrum falls off very rapidly (exponentially) as the surface wave wavelength becomes longer than that at the spectrum peak, i.e., at $q < q_p$. The spectrum decrease is much slower for the short gravity waves, i.e., at $q > q_p$ [Fig. 2(a)]. Because of the Bragg scattering condition, these properties of the wind wave spectrum are directly reflected in the spectrum of the abyssal T waves and its wind dependence.

The rms amplitude $\langle |Q_n^2| \rangle^{1/2}$ of the nth normal mode component of the T-phase field is given by Eq. (17). Figure 2(b) illustrates the wind dependence of the T-phase energy in terms of the contribution to the acoustic power flux in a normal mode from a unit area of the sea surface above the earthquake focus. In this geometry, the horizontal wave vector of the incident wave $\boldsymbol{q}_{\text{in}} = 0$ on the right side of Eq. (17). Then, the directionality of the T-phase radiation is given by the factor D_W in the wind wave spectrum [Eq. (27)]. Equation (18) shows that the wind speed dependence of the acoustic power flux in the T wave is obtained by the integrating (or averaging) of $|Q_n^2|$ over the T-wave propagation direction. In Fig. 2(b), we show the mode amplitude squared, $|Q_n^2|$, which is averaged over the statistical ensemble of fully developed wind waves. It is also averaged over the T-wave propagation direction for a given wind direction or, equivalently, over the wind direction for a given receiver position. On the other hand, it follows from Eq. (27) that after averaging over the wind direction, $\langle |Q_n^2| \rangle$ is given by Eq. (17), where $S_\eta(\xi_n \mathbf{e} - \mathbf{q}_{\text{in}}; \mathbf{r}_3)$ is replaced with $W(|\xi_n \mathbf{e} - \mathbf{q}_{\text{in}}|)$ in the integrand. Hence, the result is independent of the surface wave directionality D_W and its dependence on q in Eq. (27). Because averaging over the wind direction is equivalent to integration over the receiver azimuth, the acoustic power flux in the T waves is also independent of

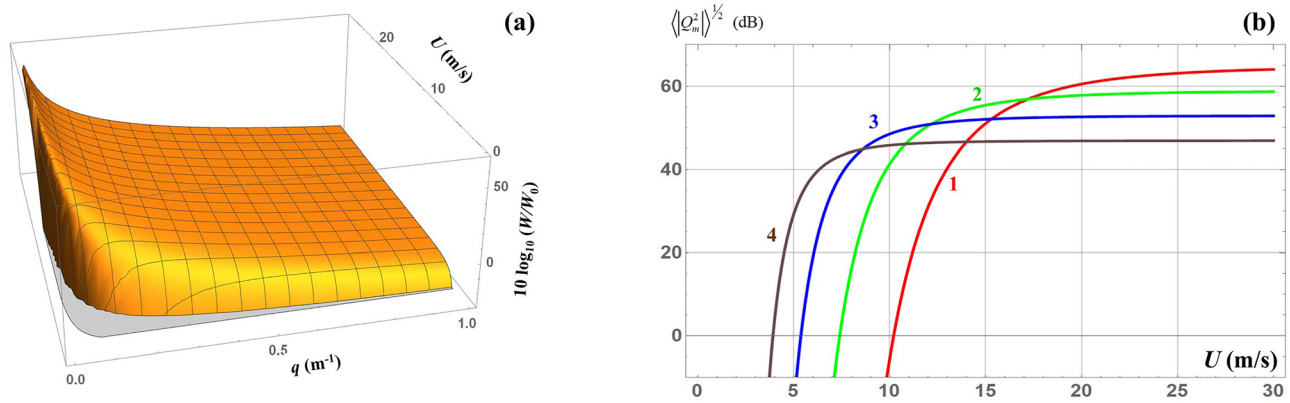

FIG. 2. (Color online) The dependence of the abyssal T-phase mode amplitude on the wind speed. (a) The azimuthally averaged Pierson-Moskovitz spectrum of the wind waves as described by Eq. (28) is shown as a function of the surface gravity wave wavenumber q and wind speed U at 19.5 m above the sea surface; $W_0 = 1\,\mathrm{m}^4$. (b) The root mean square (rms) amplitude of a normal mode of the T-waves generated by scattering on the wind seas in a unit area above the earthquake focus is shown for four frequencies: 5 Hz (1), 10 Hz (2), 20 Hz (3), and 40 Hz (4), and the mode phase speed of 1500 m/s. The mode amplitude is arbitrarily normalized assuming a frequency-independent acoustic pressure amplitude in the earthquake-generated incident wave.

D_W at the normal incidence of the ballistic waves. The numerical values of the sound frequency f, indicated in Fig. 2(b), refer to the mode with the nominal phase speed c_n of 1500 m/s. For a generic mode dispersion relation $c_n = c_n(f)$, the frequency f should be rescaled to $(1500\,\mathrm{m/s})f/c_n(f)$.

The T-phase amplitude rapidly increases with the wind speed for the weak and moderate winds and saturates at very high wind speeds [Fig. 2(b)]. The higher acoustic frequencies are more readily excited by weaker winds and saturate at smaller wind speeds. For an incident wave with a white spectrum, the higher acoustic frequencies dominate in the T-phase spectrum at low wind speeds, whereas the low frequencies prevail at strong winds. The abyssal T-phase energy and spectrum can be very sensitive to the wind speed. Away from the saturation regime, a drastic 40 dB increase in the narrowband mode amplitude requires an increase in the wind speed of just a few meters per second [Fig. 2(b)].

The spectrum of T waves at different wind speeds is further illustrated in Fig. 3. Figure 3 shows the mode amplitude squared, $|Q_n^2|$, which is averaged over the statistical ensemble of fully developed wind waves and the wind direction. Therefore, the result is independent of the wind waves directionality, which is described by the factor $D_W(q,\psi)$ in Eq. (27). Similar to Fig. 2(b), Fig. 3(a) refers to the T-phase generation at the normal incidence of the ballistic waves from the earthquake focus. Figure 3(a) shows a steady increase in the normal mode amplitudes with the wind speed in the entire range of T-phase frequencies. The most distinctive feature of the predicted T-phase spectra is a sharp low-frequency cutoff. At low acoustic frequencies, the Bragg scattering into proper normal modes of the underwater waveguide requires long wind waves with their wave vector matching the horizontal wave vector of the acoustic normal mode; see Eq. (17). For instance, the resonance scattering into the modes at 5 Hz occurs at the surface gravity waves with wavelengths of about 300 m. Thus, the low-frequency acoustic cutoff reflects the sharp drop in the wind wave spectrum at $q < q_p$. The cutoff shifts to lower acoustic frequencies and the T-phase spectrum broadens when the wind speed increases [Fig. 3(a)].

The frequency dependence of the efficiency of the T-wave generation by the scattering of obliquely incident waves is qualitatively similar to but quantitatively different from the case of normal incidence. This is illustrated in Fig. 3(b). At points on the ocean surface away from the earthquake epicenter, the T-phase is generated with different amplitudes in different horizontal propagation directions even after averaging over the wind direction [Fig. 3(b)]. For obliquely incident waves, the wind waves of different wavelength are responsible for the T waves propagating in different azimuthal directions; see Eq. (17). When the incident wave and T wave propagate in opposite horizontal directions, the low-frequency cutoff shifts somewhat toward the lower frequencies; when the propagation directions are the same, there is a more significant shift toward the higher frequencies [Fig. 3(b)].

In addition to the frequency dependence of the generation efficiency of each normal mode, illustrated in Fig. 3, the T-phase spectrum at a distant receiver is influenced by the number of propagating modes, which increases with the frequency, frequency-dependent transmission losses caused by the sound attenuation, and the spectrum of the seismic source.

B. *T*-phase excitation due to the swell

Statistically, the wave height and surface gravity wave energy are dominated by the sea swell rather than wind waves almost everywhere in the World Ocean.[45] We argue below that the swell is also expected to dominate in the generation of abyssal T waves.

The sea swell is generated by very strong winds in distant storms. Because of the pronounced dispersion of the surface gravity waves in deep water, the swell is observed at large distances from its source as a wavetrain of long gravity waves with nearly identical wavelengths. A typical width of

https://doi.org/10.1121/10.0007283

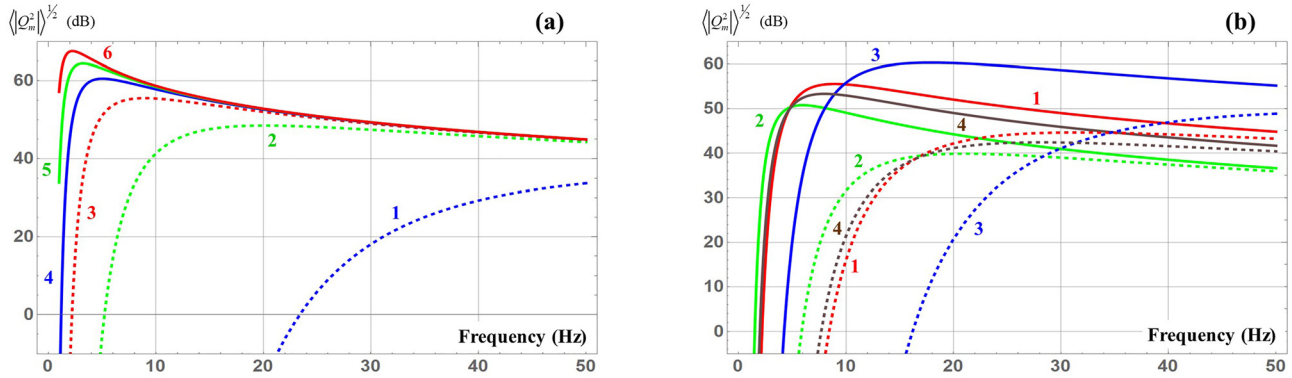

FIG. 3. (Color online) The dependence of the amplitude of a modal component of the T-wave, which is generated by scattering on the fully developed wind seas, on sound frequency and the mode propagation direction. (a) The frequency dependences of the rms amplitude of a normal mode, which is generated by scattering in a unit area above the earthquake focus, are shown for six wind speeds: 5 m/s (1), 10 m/s (2), 15 m/s (3), 20 m/s (4), 25 m/s (5), and 30 m/s (6). (b) The rms amplitude of a normal mode is shown for the scattering in a unit area above the earthquake focus (1) and away from the epicenter (2–4), where the grazing angle of the earthquake-generated incident wave is 60° at the depth, where $c(z) = c_m$. The horizontal propagation directions of the mode and incident wave are either opposite (2), the same (3), or orthogonal (4). The solid and dashed lines refer to the wind speeds of 15 m/s and 8 m/s, respectively. A nominal value of 1500 m/s is assumed for the mode phase speed c_m.

a wavetrain is several tens of wavelengths across the wavefronts with an even longer extent along the wavefronts.[61] Thus, ocean surface elevations due to the swell have a much larger correlation length then the surface roughnesses caused by wind waves. This difference has a major effect on the scattering of low-frequency sound. Although wind waves can be modeled as a random wave field, it is more appropriate to model a snapshot of the sea swell in an area of several and perhaps a few tens of kilometers as a deterministic wave field.

Unlike wind waves, there are no widely accepted swell models. We will use the following simple, idealized model to illustrate the distinctive features of the T-phase generation at the sound scattering by the swell. At the time of an earthquake, let the surface elevation η in a swell wavetrain be

$$\eta(x,y) = \sqrt{2}\sigma_\eta(y)\sin(\mu x - \mu x_0), \quad |x - x_0| < L/2, \tag{29}$$

in a region of width L in the direction of the swell propagation, which is chosen as the x coordinate axis; $\eta = 0$ at $|x - x_0| \geq L/2$. A large, integer number of swell wavelengths $2\pi/\mu$ fits in the band $|x–x_0| \leq L/2$, and $\eta(x,y)$ is a continuous function of the horizontal coordinates. The rms surface elevation σ_η is a gradually varying function of y and tends to zero at $|y - y_0| \to \infty$ such that the energy of the wavetrain is finite. The center of the swell wavetrain is at the point $(x_0,y_0,0)$, which can be located either at the earthquake epicenter (0,0,0) or away from it.

At the scattering of the ballistic sound waves [Eq. (16)] at the ocean surface with the surface elevations η [Eq. (29)], Eq. (10) for the amplitude of a T-phase modal component becomes

$$Q_n(\mathbf{r}) = \sqrt{2}\int_{x_0-L/2}^{x_0+L/2} dx_1 \sin(\mu x_1 - \mu x_0) \times \int_{-\infty}^{\infty} dy_1 \frac{\exp(i\xi_n|\mathbf{r} - \mathbf{r}_1| + i\mathbf{q}_{\text{in}}\cdot\mathbf{r}_1)}{\sqrt{|\mathbf{r} - \mathbf{r}_1|}} \times \sigma_\eta(y_1)\frac{\partial P(\mathbf{r}_1,0)}{\partial z}, \tag{30}$$

where the 2-D horizontal position vector $\mathbf{r}_1 = (x_1,y_1)$. In the integral over y_1 in Eq. (30), the integrand contains a rapidly varying exponential and slowly varying functions σ_η, $\mathbf{q}_{\text{in}} = (q_{\text{in1}},q_{\text{in2}},0)$, and $\partial P/\partial z$. The integral can be calculated by the method of stationary phase.[55] Disregarding the small derivatives of q_{in2}, the equation for the stationary point[55] $y_1 = y_{1s}$ becomes

$$\frac{y - y_{1s}}{\sqrt{(x - x_1)^2 + (y - y_{1s})^2}} = \frac{q_{in2}}{\xi_n}. \tag{31}$$

For any observation point at $|x - x_0| > L/2$, the integrand has a single stationary point. By approximating the integral over y_1 in Eq. (30) by the contribution of the stationary point,[55] we obtain

$$Q_n(\mathbf{r}) = 2\sqrt{\pi\xi_n}e^{i\pi/4}\int_{x_0-L/2}^{x_0+L/2}\frac{\sin(\mu x_1 - \mu x_0)\sigma_\eta(y_{1s})}{\sqrt{\xi_n^2 - q_{\text{in2}}^2}} \times \frac{\partial P(x_1,y_{1s},0)}{\partial z}\exp\left(i\sqrt{\xi_n^2 - q_{\text{in2}}^2}|x - x_1| + iq_{\text{in1}}x_1 + iq_{\text{in2}}y\right)dx_1. \tag{32}$$

Assuming a negligible variation of σ_η, $\mathbf{q}_{\text{in}}$, and $\partial P/\partial z$ with x_1 within the swell wavetrain, the integral on the right side of Eq. (32) is easily calculated, and we obtain

$$Q_n(\mathbf{r}) = 2e^{i\pi/4}\sqrt{\frac{\pi\xi_n}{\xi_n^2 - q_{\text{in2}}^2}}\frac{\partial P}{\partial z}\sigma_\eta L\left(\frac{\sin Y_2}{Y_2} - \frac{\sin Y_1}{Y_1}\right) \times \exp\left(i\sqrt{\xi_n^2 - q_{\text{in2}}^2}|x - x_0| + iq_{\text{in2}}y\right), \tag{33}$$

where

$$Y_j = \left[q_{\text{in1}} - \sqrt{\xi_n^2 - q_{\text{in2}}^2}\frac{x - x_0}{|x - x_0|} + (-1)^j\mu\right]\frac{L}{2}, \quad j = 1,2. \tag{34}$$

Equations (33) and (34) give the normal mode amplitudes in the abyssal T waves due to the swell at the observation points at $|x - x_0| > L/2$, i.e., outside of the swell wavetrain.

The Bragg scattering condition and the narrowband, quasiperiodic nature of the surface elevation in the swell wavetrains combine to produce the rather different dependence of the T-phase energy on the mode frequency and propagation direction than in the case of the wind waves [cf. Figs. 2(b) and 3 with Fig. 4]. Figure 4 illustrates the predictions of Eqs. (33) and (34). At a given sound frequency and normal mode propagation direction, a swell wavetrain most efficiently generates the mth normal mode at a specific grazing angle χ of the ballistic wave [Fig. 4(a)], where the secondary peaks in χ give T waves that are weaker by tens of dB [Fig. 4(a)]. The contrast between the main and subsequent peaks is controlled by the parameter $\mu L \gg 1$. The resonance value of the grazing angle χ depends on the wavetrain position relative to the epicenter via the angle between the azimuthal directions of the swell and ballistic wave propagation [Fig. 4(a)]. For the sound frequency and swell wavelength (10 Hz and 200 m) in Fig. 4(a), the resonance excitation occurs for the wavetrains away from the epicenter, where χ is between about 47° and 78°.

The T-phase spectrum and, in particular, the frequency at which a normal mode is resonantly generated, depend on the propagation directions of the ballistic wave and sea swell. It is illustrated in Fig. 4(b), where the mode amplitude is shown as a function of the frequency and grazing angle of the ballistic wave, when the sea swell travels at a 45° angle to $\mathbf{q}_{\text{in}}$. In terms of the variables Y_j introduced in Eq. (34), a resonance occurs when either $Y_1 = 0$ or $Y_2 = 0$. The T-phase spectrum and resonance frequency for each normal mode also depend on the swell wavelength $\lambda_{\text{sw}} = 2\pi/\mu$. The longer λ_{sw} favors excitation of the lower-frequency T waves ([Figs. 4(c) and 4(d)]. The same swell wavetrain generates lower-frequency T waves when it is located around the epicenter [Fig. 4(c)] than when it is located away from the epicenter [Fig. 4(d)]. If the sea swell with the same wavelength and propagation direction is present in a large area with a dimension comparable to the hypocenter depths, the resonantly excited normal mode is received at different frequencies at the observation points, which are located at different azimuthal directions from the epicenter. According to Eq. (34),

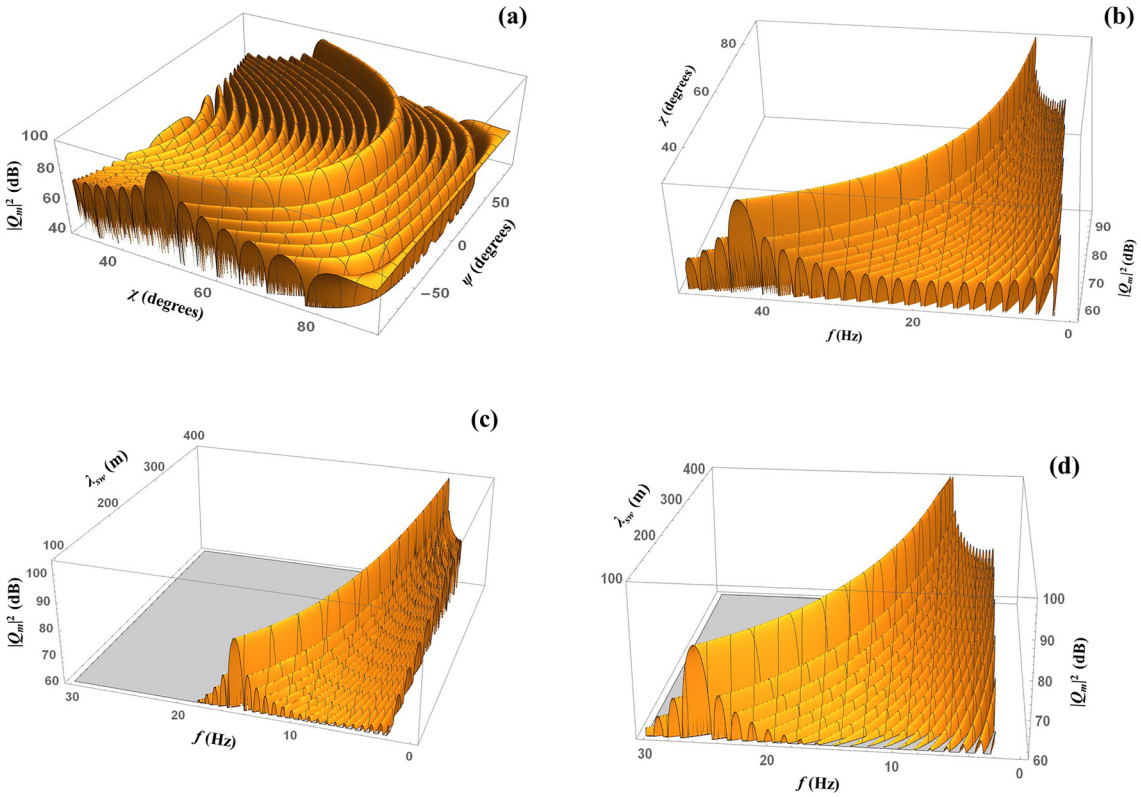

FIG. 4. (Color online) The generation of T waves at the scattering of ballistic waves from an earthquake by a wavetrain of sea swell. (a) The dependence of the amplitude of a normal-mode component of the T wave on the grazing angle χ of the incident wave at the location of the swell wavetrain and the angle ψ between the azimuthal directions of propagation of the incidence waves and swell. The sound frequency is 10 Hz. The swell wavelength $\lambda_{\text{sw}} = 200$ m. (b) The variation of the normal mode amplitude with the grazing angle of the incident waves and sound frequency when the angle between the azimuthal directions of propagation of the incidence waves and swell is 45°. The swell wavelength $\lambda_{\text{sw}} = 200$ m. (c) The dependence of the acoustic mode amplitude on the sound frequency and the wavelength of swell at normal incidence for vertically propagating ballistic waves. (d) The same as in (c) but for the swell wavetrain located away from the earthquake epicenter, $\chi = 60°$, $\psi = 45°$. A common but otherwise arbitrary normalization of the acoustic mode amplitude is used in all of the panels. The width of the swell wavetrain in the direction of its propagation equals 20 swell wavelengths. A nominal value of 1500 m/s is assumed for the phase speed c_m of the acoustic normal mode. The numerical values of the grazing angle of the earthquake-generated incident waves refer to the depth, where $c(z) = c_m$.

https://doi.org/10.1121/10.0007283

note also that any swell wavetrain resonantly scatters the ballistic waves of the compressional and shear-wave origin in different azimuthal directions and at different frequencies.

According to Eqs. (33) and (34), the magnitude squared of the amplitude of the nth normal mode generated at the scattering by the sea swell is

$$|Q_n^2| = \frac{32\pi^3\xi_n}{\xi_n^2 - q_{\text{in2}}^2}\left|\frac{\partial P}{\partial z}\right|^2\left|\Phi\left(q_{\text{in1}} - \sqrt{\xi_n^2 - q_{\text{in2}}^2}\,\frac{x - x_0}{|x - x_0|}\right)\right|^2, \tag{35}$$

where

$$\Phi(q_1) = \frac{iL\sigma_\eta}{2^{3/2}\pi}e^{-iq_1x_0}\frac{\sin Y}{Y}\Bigg|_{Y=(q_1-\mu)L/2}^{Y=(q_1+\mu)L/2} \tag{36}$$

is the one-dimensional wavenumber spectrum of the surface elevation due to the swell [Eq. (29)] viewed as a function of x. We show below that the same result for $|Q_n^2|$ can be formally obtained from the results, which have been derived in Sec. II B for the random sea surface roughness, if one uses

$$S_\eta(q_1, q_2) = \frac{8\pi}{L}|\Phi(q_1)|^2\delta(q_2) \tag{37}$$

for the swell power spectrum in Eq. (17). Here, $\delta(\cdot)$ denotes the Dirac delta function. It originates from the surface elevation being independent of the coordinate y. We assume, here, that σ_η is independent of the coordinates. We will also assume for simplicity that the variations of $\mathbf{q}_{\text{in}}$ and $\partial P/\partial z$ in the incident wave are negligible within the swell wavetrain.

In the integrand on the right side of Eq. (17), $q_2 = \xi_n(y - y_3)|\mathbf{r} - \mathbf{r}_3|^{-1} - q_{\text{in2}}$ and $q_2 = 0$ when $y_3 = y_{1s}$; see Eq. (31). Then, $|\mathbf{r} - \mathbf{r}_3| = |x - x_3|(1 - \xi_n^{-2}q_{\text{in2}}^2)^{-1/2}$ and

$$\begin{aligned}\delta(q_2) &= \left|\frac{\partial}{\partial y_3}\left(\xi_n\frac{y - y_3}{|\mathbf{r} - \mathbf{r}_3|} - q_{\text{in2}}\right)\right|^{-1}\delta(y_3 - y_{1s}) \\ &= \frac{\xi_n^2|x - x_3|}{\left(\xi_n^2 - q_{\text{in2}}^2\right)^{3/2}}\delta(y_3 - y_{1s}).\end{aligned} \tag{38}$$

Inserting Eqs. (37) and (38) in the integrand in Eq. (17) and integrating first over y_3 and then over x_3, gives Eq. (35). Note that this derivation of Eq. (35), like Eq. (17), applies in the far field with respect to the correlation scale of the sea surface roughness. This is a very significant limitation in the case of the swell. No such assumption was made in the derivation of Eq. (33), which is applicable everywhere outside of the swell wavetrain itself.

To elucidate the relative significance of the wind seas and swell in the abyssal T-wave problem, let us compare the acoustic power fluxes J_n in the normal modes generated at sound scattering by two types of ocean surface roughness in the same area $|x - x_0| \le L/2$ of the ocean surface. For simplicity, we will disregard the dependence of $\partial P/\partial z$ on x and the variation of $\mathbf{q}_{\text{in}}$ and the wind wave spectrum with coordinates within the area that contributes the most to the scattering. Then, Eq. (19) gives

$$\langle J_n\rangle = \frac{\pi^2 E}{2\omega}L\tilde{S}_\eta, \quad E = \left(\frac{1}{\rho}\frac{\partial f_n}{\partial z}\right)_{z=0}^2\int_{-\infty}^{+\infty}\left|\frac{\partial P}{\partial z}\right|^2 dy \tag{39}$$

for the wind seas. Here, $\tilde{S}_\eta$ is the value of the wind wave spectrum at some point within the integration domain in Eq. (19). [Equation (39) follows immediately from application of the first mean value theorem for integrals to the right side of Eq. (19).] $\tilde{S}_\eta$ in Eq. (39) can be viewed as a weighted average of the spectrum S_η over the horizontal direction of the mode propagation within the interval $|\xi_n - q_{\text{in}}| < q < \xi_n + q_{\text{in}}$ of the wavenumbers q of the wind seas. This interval contains all of the possible $q = |\xi_n\mathbf{e} - \mathbf{q}_{\text{in}}|$ in the integrand in Eq. (19). When the peak $q = q_p$ of the wave spectrum lies within the interval $|\xi_n - q_{\text{in}}| < q < \xi_n + q_{\text{in}}$, $\tilde{S}_\eta \sim q_p^{-2}\sigma_\eta^2/2\pi$, according to Eqs. (27) and (28); $\tilde{S}_\eta$ is small otherwise.

For the scattering by the swell, the acoustic power flux in a normal mode can be calculated by integrating the x component of the acoustic power flux density along the vertical planes $x - x_0 = \text{const.} > L/2$ (toward increasing x) and $x - x_0 = \text{const.} < -L/2$ (toward decreasing x). Similar to the derivation of Eq. (18), from Eqs. (9) and (33), we find

$$\begin{aligned}J_n = &\frac{\xi_n L^2}{16\omega\left(\xi_n^2 - q_{\text{in2}}^2\right)}\left(\frac{1}{\rho}\frac{\partial f_n}{\partial z}\right)_{z=0}^2 \\ &\times\int_{-\infty}^{+\infty}\sigma_\eta^2\left(\frac{\sin Y_2}{Y_2} - \frac{\sin Y_1}{Y_1}\right)^2\left|\frac{\partial P}{\partial z}\right|^2 dy\end{aligned} \tag{40}$$

for the power flux toward increasing x. $Y_{1,2}$ in Eq. (40) are given by Eq. (34) with $(x - x_0)/|x - x_0| = 1$. The power flux toward decreasing x is given by the same Eq. (40) but now with $(x - x_0)/|x - x_0| = -1$ in Eq. (34) for $Y_{1,2}$.

The resonant excitation of the nth acoustic normal mode at the scattering by the swell occurs when one of the four conditions, $q_{\text{in1}} \pm \sqrt{\xi_n^2 - q_{\text{in2}}^2} \pm \mu = 0$, is met. Then, one of the $Y_{1,2}$ values in Eq. (40) is zero. Near the resonance frequency [more specifically, as long as $|Y_{1,2}|$ is either small or $O(1)$], the term in parenthesis in the integrand on the right side of Eq. (40) is $O(1)$, and $J_n \sim EL^2\sigma_\eta^2/8\omega\xi_n$. Note that J_n is proportional to L^2 because of the coherent scattering of sound by the swell wavetrain. Away from the resonance frequencies, when all $|Y_j| \gg 1$, J_n decreases by the factor on the order of $\mu^2L^2 \gg 1$. For the contribution of the wind seas, Eq. (39) gives $\langle J_n\rangle \sim \pi EL\sigma_\eta^2/2\omega\xi_n^2$ when the peak of the wind wave spectrum fully contributes to generation of the nth normal mode. As expected, $\langle J_n\rangle$ is proportional to the area occupied by the surface roughness and, hence, L at the incoherent scattering of sound by the random surface waves.

Aside from the roughly estimated numerical factors in the vicinity of the resonance frequencies, the energy of the swell contribution to the T-phase exceeds the maximum

contribution of the wind waves with the same wave heights by the factor $\xi_n L \gg 1$. Thus, T waves caused by the swell can dominate over the wind-wave contribution in the narrow frequency bands not only in specific directions but also in the azimuthally integrated power flux, even when the local winds are strong and the peak of the wind wave spectrum $q_p \sim \mu$. However, according to Eq. (40), only a narrow vicinity $\delta f \sim c/L$ of the resonant frequency contributes significantly to the energy of the sound scattered by the swell, and the broadband acoustic power fluxes resulting from the scattering by the wind waves and swell with the same wave heights prove to be comparable.

C. Dependence of *T*-phase energy and duration on the hypocenter depth

The calculation of the T-wave spectrum with Eqs. (17) and (33) requires knowledge of the distribution of the wind speed and sea swell in an area around the earthquake epicenter as well as a model of the ballistic waves generated by the earthquake. In this section, we use a basic model of the seabed and simplified, semiquantitative versions of the theoretical results for the mode amplitudes to estimate the dimensions of the area of the ocean surface, where T waves are generated, and understand the variation of the abyssal T-phase duration and energy with the depth of the earthquake focus. For these estimates, the seabed is modeled as a homogeneous solid half-space with the density and elastic parameters of the Earth's crust near the earthquake focus, and a compact, directional seismic source is supposed to be located at the focus. For orientation, $c_l = 8$ km/s, $c_t = 4$ km/s, and $M = 3$ can serve as the representative values of the compressional and shear wave speeds and the ratio of the densities of Earth's crust and sea water, respectively. The hypocenter (focus) of the earthquake is at the point $(0,0,H+D)$ at a depth D below the seafloor (Fig. 1). The source will be characterized by the frequency-dependent amplitudes A_P and A_{SV} and corresponding directional factors $B_P(\theta, \varphi)$ and $B_{SV}(\theta, \varphi)$ of the compressional (P) and vertically polarized shear (SV) waves that are radiated by the earthquake. Horizontally polarized shear waves in the crust do not contribute to the acoustic field in water.[62] By definition, $|B_P| \le 1$ and $|B_{SV}| \le 1$. When considering the incident waves that are scattered at the ocean surface, we focus on the ballistic waves arriving directly from the source and disregard the weaker arrivals, which reach the ocean surface and are scattered after previously undergoing surface and bottom reflections.

The parameters of the incident acoustic wave, which is scattered by the rough ocean surface, affect the wind-wave contribution to the T-phase mode amplitudes [Eq. (17)] via $\partial P/\partial z$ and $\mathbf{q}_{\text{in}}$. The amplitude and angle of incidence of the incident wave vary along the ocean surface. With the wind waves being independent from the focal depth and other earthquake properties, after averaging over the wind speeds and directions, Eq. (17) can be written as $\langle |Q_n^2| \rangle = 4\pi^2 r^{-1} \langle S_\eta \rangle \Psi$, where

$$\Psi = \int |\partial P(\mathbf{r}_3, 0)/\partial z|^2 d\mathbf{r}_3. \tag{41}$$

The average $\langle S_\eta \rangle$ of the wind wave spectrum is largely insensitive to the angle of incidence of the ballistic waves from the earthquake. For instance, it follows from Eqs. (27) and (28) that $\langle S_\eta \rangle \sim q_p^{-2} \sigma_\eta^2 / 2\pi$ and is controlled by the representative wind speed alone when the peak of the wind wave spectrum contributes to the T-phase generation. Hence, the effect of the earthquake parameters on the T-phase generation is characterized by the surface integral Ψ in Eq. (41).

Averaging Eq. (40) over the swell wavelength and wavetrains' location and propagation direction shows that Ψ [Eq. (41)] also encapsulates the effect of the incident wave on the T-phase generation caused by the sound scattering by the sea swell.

For the steep angles at which ballistic waves from the earthquake propagate in the water column, variations of the sound speed in water with the depth are insignificant. The sound speed c and density ρ in water will be assumed constant in the analysis of the ballistic waves. Then, using the results for the spherical wave transmission through a plane interface of two homogeneous media,[55] we find

$$\frac{\partial P(\mathbf{r}, 0)}{\partial z} = -\frac{i\omega}{c} A_P B_P(\theta_l, \varphi) T_l(\theta_l) \times \left[\frac{\sin\theta_l}{r} \Big/ \left(\frac{D}{\cos^3\theta_l} + \frac{cH}{c_l \cos^3\theta} \right) \right]^{1/2} \times \exp\left[i\omega \left(\frac{D}{c_l} \cos\theta_l + \frac{H}{c} \cos\theta \right) - \frac{\alpha_l D}{\cos\theta_l} \right] \tag{42}$$

at the point $\mathbf{r} = r(\cos\varphi, \sin\varphi, 0)$ on the ocean surface. Equation (42) describes the contribution of the compressional waves in the seabed and is obtained in the ray approximation. Here, θ and θ_l are the incidence angles (i.e., the angle that the ray makes with the z axis) in the ocean and seabed, respectively; α_l denotes the attenuation coefficient of the compressional waves, and T_l is the plane wave transmission coefficient of the compressional waves at the seafloor. The incident angles are related by Snell's law and can be found from the equations

$$c^{-1} \sin\theta = c_l^{-1} \sin\theta_l, \quad r = H \tan\theta + D \tan\theta_l. \tag{43}$$

When r increases from zero to infinity, θ_l increases from zero to $\pi/2$, according to Eq. (43), whereas θ increases from zero to $\arcsin(c/c_l)$. The horizontal wave vector $\mathbf{q}_{\text{in}}$, which enters Eqs. (16), (17), and (33), is $\mathbf{q}_{\text{in}} = \omega c^{-1} \sin\theta (\cos\varphi, \sin\varphi, 0)$.

The contribution of the shear waves in the seabed into $\partial P/\partial z$ at the ocean surface is given by equations similar to Eqs. (42) and (43), except the SV wave source amplitude A_{SV}, directional factor B_{SV}, and attenuation coefficient α_t should be used instead of A_P, B_P, and α_l, respectively.

https://doi.org/10.1121/10.0007283

The transmission coefficient T_t of the SV waves replaces T_l in Eq. (42). In addition, the shear wave speed c_t and incidence angle θ_t should be used instead of c_l and θ_l, respectively, in Eqs. (42) and (43). Because $c_l > c_t$, it follows from Eq. (43) that at any $r > 0$, the ballistic waves resulting from the compressional waves in the seabed arrive at the sea surface at steeper angles than the ballistic waves resulting from the shear waves radiated by the earthquake.

In the case of fluid–fluid interfaces, the transmission coefficient[62]

$$T_l(\theta_l) = 2c\ \cos\ \theta_l/(c\ \cos\ \theta_l + Mc_l \cos\ \theta). \tag{44}$$

At a solid–fluid interface, T_l and T_t are given by more cumbersome equations,[62] but as in Eq. (44), T_l is proportional to $\cos\ \theta_l$ and vanishes when $\theta_l \to \pi/2$, whereas T_t is proportional to $\cos\ \theta_t$ and vanishes when $\theta_t \to \pi/2$; see Eqs. (4.2.37)–(4.2.42) in Ref. 62. These properties of the transmission coefficients ensure that the areas far from the epicenter contribute little to the T-wave generation. The transmission coefficients $T_l\ (\theta_l)$ and $T_t\ (\theta_t)$ have $O(1)$ values for all real θ_l and θ_t, respectively; $T_t\ (0) = 0$ and $T_t\ (0)$ is nonzero.

Because the ballistic waves originating from the compressional and shear waves in the seabed have distinct horizontal wave vectors $\mathbf{q}_{\text{in}}$, the integral Ψ in Eq. (41) should be calculated separately for these incident waves. [The $\mathbf{q}_{\text{in}}$ values are close at near-normal incidence of the ballistic waves, which occurs in the vicinity $r \ll H + D$ of the epicenter. However, because $T_t\ (0) = 0$, the amplitude is then negligible of the incident wave caused by the SV waves in the bottom, and interference of the two incident waves has no effect on the T-wave generation.] For the compressional wave contribution from Eqs. (41)–(43), we find

$$\Psi_P = \left|\frac{\omega}{c}A_P\right|^2 \int_{-\pi}^{\pi} \frac{d\varphi}{2} \int_0^{\pi/2} |B_P(\theta_l, \varphi) T_l(\theta_l)|^2 \times \exp\left(-\frac{2\alpha_l D}{\cos\ \theta_l}\right) \sin\ 2\theta_l\, d\theta_l. \tag{45}$$

Equation (43) has been used to change the integration variable in Eq. (41) from r_3 to θ_l. The result for the contribution Ψ_{SV} of the shear waves in the seabed differs from Eq. (45) by the obvious change of notations, which has been discussed above for Eq. (42).

Note that Eq. (45) does not contain the ocean depth H. The hypocenter depth D enters Eq. (45) only via the exponential term that describes the wave attenuation in the solid bottom. Thus, our estimates show that the energy of the abyssal T waves is independent of the ocean depth and insensitive to the hypocenter depth at such frequencies where the wave energy dissipation is weak. This finding is not restricted to the basic ocean and Earth's crust model that we consider and by changing the integration variables to ray launch angles, can be extended to the stratified seabed as long as the ray-theoretical description of the ballistic waves remains applicable.

The independence or lack of sensitivity of the abyssal T-wave energy to H and D appears counterintuitive at first. Indeed, according to Eq. (42), the amplitudes of the incident waves on the ocean surface rapidly decrease with increasing H and D. However, the decrease in the amplitude is compensated by an increase in the ocean surface area that contributes to the T-wave generation. For instance, if H and D are increased by the same factor $\beta > 1$ and the ray launch angle θ_l (or θ_t) is kept constant, r in Eq. (43) will increase by the same factor β. The incident wave amplitude in Eq. (42) is decreased by the factor β as long as the wave dissipation is negligible. The decrease in the integrand in the surface integral for Ψ in Eq. (41) by the factor β^2 is exactly compensated by the increase in $d\mathbf{r}_3 = r_3 dr_3 d\varphi$. This is closely related to the fact that as long as the dissipation is negligible, the energy of the body waves (as opposed to the interface seismo-acoustic waves) reaching the ocean surface remains unchanged when the depth of a compact seismic source varies.

In addition to the T-phase energy, the signal duration is another important characteristic of T waves. At distant receivers, T-phase duration is controlled by the seismic event (rupture) duration in the earthquake focus, normal mode dispersion in the oceanic waveguide, and linear dimensions of the region where the T waves are generated. The generation of T waves caused by sound scattering occurs with a different efficiency at various points on the ocean surface and tends to gradually decrease with the distance from the epicenter. Assuming spatially uniform statistics of the surface gravity waves, the effective radius r_g of the area around the epicenter, where the abyssal T waves are generated, can be estimated as follows [cf. Eq. (41)]:

$$r_g = \Psi^{-1} \int r |\partial P(\mathbf{r}, 0)/\partial z|^2 d\mathbf{r}. \tag{46}$$

Much like Ψ_P and Ψ_{SV} above, r_g needs to be estimated separately for the incident waves caused by the P and SV waves in the seabed. In terms of r_g, the lower bound of the T-phase duration can be roughly estimated as the difference $2r_g/c$ of the acoustic travel times from the opposite margins of the region where the T waves are generated. Similarly, r_g/c provides an estimate of the rise (onset) time of the envelope of the T-phase waveform.

For the ballistic waves resulting from the P waves in the seabed, from Eqs. (42), (43), and (46), we find

$$r_g = \left|\frac{\omega}{c}A_P\right|^2 \Psi_P^{-1} \int_{-\pi}^{\pi} d\varphi \int_0^{\pi/2} |B_P(\theta_l, \varphi) T_l(\theta_l)|^2 \times \left(\frac{H\ \cos\ \theta_l}{\sqrt{c_l^2 c^{-2} - \sin^2\theta_l}} + D\right) \times \exp\left(-\frac{2\alpha_l D}{\cos\ \theta_l}\right) \sin^2\theta_l\, d\theta_l. \tag{47}$$

The derivation of Eq. (47) is quite similar to that of Eq. (45). For the ballistic wave resulting from the SV waves in

the seabed, the result follows from Eq. (47) after the previously discussed change in notation. The integral on the right side of Eq. (47) and Ψ_P depend on the source directionality and environmental parameters. In the case of an omnidirectional source in a homogeneous medium ($c = c_l$, $T_l \equiv 1$) without dissipation, Eqs. (45) and (47) give $r_g = 0.5\pi(H+D)$. We now show that r_g remains on the order of $H+D$ in the general case with a possible exception for high frequencies.

Note that the integrands in Eqs. (45) and (47) are small when either $\sin\theta_l \ll 1$ (because of the factors $\sin 2\theta_l$ and $\sin^2\theta_l$, respectively) or $\cos\theta_l \ll 1$ (because of the transmission coefficient). Hence, $\tan\theta_l = O(1)$ in the range of θ_l that contributes most to the integrals. The integrand in Eq. (47) differs from the integrand in Eq. (45) by the factor $r = H\tan\theta + D\tan\theta_l$, which is on the order of $H+D$, when $\tan\theta_l = O(1)$. Thus, $r_g = O(H+D)$ generally, and our estimates indicate a longer abyssal T-phase duration for deeper earthquakes. At sufficiently high frequencies, i.e., when waves are strongly dissipated in the seabed over the path of length D, the exponential factor $\exp(-2\alpha_l D/\cos\theta_l)$ in the integrands of Eqs. (45) and (47) favors a small θ_l. It results in smaller r_g values at higher T-wave frequencies than at lower T-wave frequencies.

Our results indicate, in agreement with the observations,[63–66] that the T-phase rise (onset) time increases with the hypocenter depth D. Furthermore, r_g and the rise (onset) time increase with the water depth H. This prediction is opposite to that of the seafloor scattering model by de Groot-Hedlin and Orcutt[40] but agrees with the observations analyzed by Williams *et al.*[2]

IV. DISCUSSION

A. Comparison to other mechanisms of *T*-phase generation

For the scattering of ballistic waves by a rough ocean surface to be a significant mechanism of T-phase generation, the resulting T waves should have a sufficiently large amplitude. At the very least, surface scattering should excite the acoustic normal modes much more efficiently than these are excited in a horizontally stratified ocean with the plane, horizontal boundaries and interfaces.

The direct excitation of the T waves, which have phase and group speeds close to the sound speed c in water, by seismic sources in a layered media is very weak because of the exponential attenuation of the shape functions of the corresponding normal modes in the seabed.[1,3,41] For a rough semiquantitative estimate of the direct excitation, we model the seabed as a homogeneous fluid half-space with the sound speed $c_b > c$. The seismic wave source is modeled as a point monopole acoustic source with $A = A_0\delta(x)\,\delta(y)\,\delta(z-D)$ in Eq. (3). (The conclusions remain essentially unchanged for the more complicated dipole or quadrupole sources.) From Eqs. (2), (3), and (6), we find that the power flux $J_n^{(D)} = \omega|A_0^2|f_n^2(H+D)/8$ in the nth mode, generated in a layered medium by a point source at the earthquake focus. Here, A_0 is the source amplitude. The acoustic pressure is evanescent in the seabed: $f_n(H+D) = f_n(H)\exp\left(-\omega D\sqrt{c_n^{-2}-c_b^{-2}}\right)$, where $f_n(H)$ can be estimated from Eq. (7): $f_n^2(H) \lesssim 2\rho(0)/H$. When estimating $J_n^{(D)}$, one has to use the shear wave speed rather than the larger compressional wave speed for c_b because the evanescent shear waves attenuate more slowly below the seafloor and provide a stronger coupling of the seismic source to the normal modes that we consider [i.e., a larger value of $f_n(H+D)$].

The resulting expression for the power flux in the normal mode directly excited by the seismic source should be compared to the power flux in the same mode excited due to the scattering of ballistic waves at the rough ocean surface. To estimate the average power flux $J_n^{(W)}$ caused by the scattering by the wind waves on the ocean surface, we employ Eq. (19) and the estimates of the spatial average of the surface roughness spectrum $\langle S_\eta\rangle \sim q_p^{-2}\sigma_\eta^2/2\pi = (0.091)^2\sigma_\eta^4/2\pi$ (Secs. III A and III C) and the radius of the contributing region on the ocean surface $r_g \sim H+D$ (Sec. III C). For the modal power flux resulting from the scattering by the wind waves, we arrive at the estimate

$$J_n^{(W)} \sim \frac{\pi^2\omega\sigma_\eta^4(H+D)^2\sin^2\chi_n}{2(0.091)^2\rho(0)c^2(0)H}\left|\frac{\partial P}{\partial z}\right|_{z=0}\Bigg|^2. \tag{48}$$

In terms of the amplitude A_0 of the omnidirectional point source, for the ballistic waves on the ocean surface at the epicenter, we have $|\partial P/\partial z| \simeq \omega^2\rho_b T(0)|A_0|/4\pi(H+D)$, where $\rho_b = M\rho(0)$ is the seabed density and T is the transmission coefficient [Eq. (44)].

Combining the above estimates, we find that

$$F_1 = \frac{J_n^{(W)}}{J_n^{(D)}} \sim \frac{\sin^2\chi_n}{2(0.091)^2}\left(\frac{\omega\sigma_\eta}{c(0)}\right)^4\left[\frac{Mc(H)}{c(H)+Mc_b}\right]^2 \times \exp\left(2\omega D\sqrt{c_n^{-2}-c_b^{-2}}\right) \tag{49}$$

for the ratio of the acoustic power fluxes in the T waves at the surface scattering and direct excitation in the layered waveguide. The ratio F_1 characterizes the relative significance of the scattering by the wind waves compared to the direct excitation. Note that F_1 rapidly increases with the sound frequency, roughness amplitude, and earthquake focus depth. With $\chi_n \cong 0.1$ rad, $c_n \cong 1500$ m/s, and $c_b \cong 4000$ m/s, Eq. (49) predicts that the scattering caused by the wind waves generates T waves *hundreds of dBs* stronger than the direct excitation at frequencies as low as 1 Hz and rms surface elevations as small as $\sigma_\eta = 0.3$ m even for rather shallow earthquakes with $D = 10$ km (or at 2 Hz with even smaller $D = 5$ km). Thus, the excitation resulting from the surface scattering of the ballistic body waves dominates over the direct excitation at all of the T-phase frequencies as expected.

In a full-wave, 2-D SPECFEM (Spectral Finite Element Method) simulation, Bottero[8] compared the T-phase generation at a large-scale bathymetric feature (a 6 km-long, 12°

https://doi.org/10.1121/10.0007283

bottom slope centered on the earthquake epicenter) with contributions due to the sound scattering by a compact scatterer on the ocean surface. The scatterer was intended to roughly represent a large commercial vessel. Bottero found that in his model, the compact surface scatterers ("ships") were as strong a T-wave source as the downslope conversion on the large bathymetric feature.[8] Although the target strength of the scatterer in Ref. 8 is much larger than that of the actual ships of the same dimensions,[67] the full-wave simulation results[8] are extremely valuable as the first rigorous comparison of the efficiency of the surface scattering and downslope conversion as the T-phase sources. By an analytic evaluation of the T-phase generation by the compact scatterer considered in Ref. 8 and the wind waves, the numerical results[8] have been used to demonstrate[67] that the sound scattering by the wind waves dwarfs the contribution of the scattering by the ships in 3-D and can generate T waves at least as efficiently as the presumably dominant[3] generation mechanism of the downslope conversion on large bathymetric features.

We now provide a direct, semiquantitative comparison of the energy of the T waves that are generated in a 3-D ocean by either a large bathymetric feature (a seamount) or sound scattering caused by the gravity waves on the ocean surface. Let an isolated seamount or a small island be located at a distance R from the epicenter. The seamount rises from the otherwise horizontal seafloor to the ocean surface. The width of the seamount in the azimuthal direction is l. It is small compared to R and large compared to the water depth H and acoustic wavelengths in the T-wave frequency band. The surface of the seamount makes an angle γ with the horizontal plane. The amplitude of the normal component of the oscillatory velocity of the surface of the seamount differs from the velocity amplitude in the ballistic waves at the ocean surface at the epicenter by the factor $w > 0$, which includes the effects of the geometric spreading and wave attenuation in the bottom. For a seamount at range $R \gg D + H$ from the epicenter, the ratio of the ballistic wave amplitudes at the seamount and on the ocean surface at the epicenter $w \sim \exp(-\alpha R)(H + D)/R$, where α stands for the attenuation coefficient of the P or S waves in the seabed.

Consider the vertical cross section of the ocean from its surface to the foot of the seamount where it meets the horizontal seafloor. In this cross section, the horizontal component of the particle velocity due to the seismic waves of frequency ω in the seamount can be estimated as

$$v_1 = \frac{2w \sin\gamma}{\omega\rho}\left|\frac{\partial P}{\partial z}\right| \times \exp\left[i\Phi(z) + i\sqrt{\omega^2 c^{-2} - \beta^2}(H - z)\cot\gamma\right]\sin\beta z,$$

where the factor $2i \sin \beta z$ accounts for the interference of the incident and surface reflected acoustic waves with the vertical wavenumber β, Φ describes the variation of the phase of the seismic waves along the seamount slope, and $\partial P/\partial z$ is evaluated on the ocean surface at the earthquake's epicenter. Using the normal mode orthogonality to find the modal components of the horizontal velocity, we obtain

$$J_n^{(\mathrm{SM})} = \frac{4w^2 l \sin^2\gamma}{\omega\xi_n\rho(0)}\left|\frac{\partial P}{\partial z}\right|^2 |U_n^2|, \tag{50}$$

$$U_n = \sqrt{\rho(0)}\int_0^H dz \frac{f_n \sin\beta z}{\rho} \times \exp\left[i\Phi + i\sqrt{\omega^2 c^{-2} - \beta^2}(H - z)\cot\gamma\right] \tag{51}$$

for the acoustic power flux in the nth mode, generated by the oscillations of the seamount surface. Here, we disregarded guided acoustic mode penetration into the seabed and used the mode normalization condition Eq. (7).

Using the Cauchy–Schwarz inequality and normalization condition [Eq. (7)], the upper bound of the integral U_n [Eq. (51)] can be estimated as $|U_n^2| \le \rho(0)\int_0^H dz\rho^{-1}\sin^2\beta z \simeq H/2$. A more accurate estimate of U_n, which accounts for the oscillations of the integrand with z, is

$$|U_n| \sim 2^{-1/2}\left(\omega^2 c^{-2}(0) - \xi_n^2\right)^{-1/4} = \left[2\omega c^{-1}(0)\sin\chi_n\right]^{-1/2}, \tag{52}$$

where χ_n is the grazing angle at the ocean surface. The estimate [Eq. (52)] refers to the modes with significant amplitudes throughout the water column. At higher frequencies, there may be modes with deep turning points, which are very weakly manifested at the ocean surface and seafloor. These normal modes are not considered here.

From Eqs. (48), (50) and (52), we find that

$$F_2 = \frac{J_n^{(W)}}{J_n^{(\mathrm{SM})}} \sim \frac{\pi^2 R^2 \exp(2\alpha R)\sin^3\chi_n}{4(0.091)^2 lH\sin^2\gamma}\left(\frac{\omega\sigma_\eta}{c(0)}\right)^4 \tag{53}$$

for the ratio of the modal power fluxes resulting from the surface scattering and the seamount. The ratio increases with the range R, surface roughness, and, in agreement with the observations,[32] the T-wave frequency. It is larger for the steeper normal modes (larger χ_n) and smaller for the bigger (larger l) and steeper (larger γ) seamounts.

Depending on the environmental parameters and the wave frequency, F_2 can be large (i.e., the surface scattering dominates) or small (i.e., the contribution of the surface scattering is negligible) compared to unity. Let $\chi_n = 0.1$, $\gamma = 0.4$, $H = 4$ km, the angular azimuthal dimension of the seamount as seen from the epicenter $l/R = 0.1$, and the rms surface elevation $\sigma_\eta = 1$ m. (All angles are in radians.) To estimate the attenuation coefficient, we use a compressional wave speed of 8 km/s and Q-factor of 400.[68,69] [The attenuation coefficient equals 27.3 Q_P^{-1} dB per wavelength in a wave with the quality factor Q_P.] Then, according to Eq. (53), the surface scattering creates T waves as strong as those resulting from a seamount at the range $R = 400$ km from the epicenter at the frequency of about 5.0 Hz, while

the surface scattering is the stronger T-wave source at higher frequencies. For $R = 600$, 300, 200, and 100, the transition frequency at which $F_2 = 1$ shifts to about 3.7, 6.2, 8.3, and 13.5 Hz, respectively.

Because of their shorter wavelength and smaller quality factors, the attenuation in the seabed plays a bigger role for the shear waves than the compressional waves. Therefore, the ratio F_2 [Eq. (53)] is larger for the shear-wave contributions of the seamount oscillations. Let the shear wave speed and Q-factor be 4 km/s and 200, respectively. Then, Eq. (53) gives rather low transition frequencies of 5.6, 3.3, and 2.4 Hz for $R = 100$, 200, and 300 km, respectively.

It should be emphasized that Eq. (53) provides an estimate rather than an accurate prediction of the relative significance of the surface scattering and a large topographic feature as the T-wave sources. On the other hand, our estimates of the contribution of the surface scattering are conservative in the sense that the sea swell is expected to contribute to the T-wave generation at least as much as the wind waves (Sec. III B), and typical values of σ_η are larger for most of the World Ocean[45] than the 1 m assumed in our estimates.

Thus, the scattering by the surface gravity waves is expected to provide a significant contribution to the T-phase energy, which is comparable to the contribution resulting from a downslope conversion on a seamount. In addition, being generated around the earthquake epicenter, the surface scattering contribution will generally separate from the bathymetric contributions by its arrival time and azimuth.

B. Extensions of the theory

In Secs. II and III, we have assumed that the ocean is range independent when averaged over the time-dependent variations caused by the surface and internal gravity waves. This assumption may be too restrictive for the entire propagation path to distant receivers from the abyssal T-wave generation site in the vicinity of the earthquake epicenter. However, the assumption is sufficient to evaluate the acoustic energy of the abyssal T waves and its modal distribution in the real ocean. Indeed, outside of the relatively small region where the T waves are generated, the acoustic energy of the scattered wave is conserved and is the same in the near field as in the far field as long as the acoustic dissipation is negligible. The normal-mode distribution of the T-phase energy also remains unchanged in the horizontally inhomogeneous ocean as long as the adiabatic approximation[55] is applicable. After the normal mode amplitudes in the T-phase spectrum are calculated as described in Secs. II–III, the field can be readily propagated to long ranges with a full account of the sound absorption using the adiabatic approximation, the coupled-mode, or the parabolic-equation propagation models.

We have focused on the contributions of gravity waves in the ocean in the T-phase generation. However, the theory of excitation of the normal modes of the oceanic waveguide by the scattering of body waves, as expressed by Eqs. (10), (17), and (26), can be applied to other types of surface and volume scatterers. One important application is to the T-phase generation at the scattering by volume inhomogeneities within the seabed and roughness of the seafloor and sediment layer interfaces. This T-phase excitation mechanism has been previously considered[41,42] for the coupling within the discrete spectrum of the seismo-acoustic field. Arguably, the continuous spectrum (ballistic body waves) make a stronger contribution to the T-wave excitation by bottom scattering than the directly excited discrete spectrum modes, especially for earthquakes with deeper foci. The application of the theory developed in this paper would allow one to better constrain the effective sources of the T waves on the seafloor and within the seabed (including their spatial distribution, directionality, and frequency dependence), which were either not related quantitatively to the environmental properties[41] or arbitrarily assigned[22,39,40] in the previous work.

Our finding that the contribution of the ballistic waves scattering by the internal gravity waves into T-phase generation is negligible compared to the contribution of the ocean surface roughness does not necessarily mean that the volume scattering in the water column plays no role in this problem. At long-range propagation, internal waves contribute to the coupling of the modes generated by the surface scattering to the modes confined in the SOFAR channel. Furthermore, the water column contains many different types of inhomogeneities in a wide range of spatial scales. The scattering of the infrasound generated by air guns from the thermohaline fine structure is successfully used in seismic oceanography to measure the physical parameters of the water column.[70,71] The frequency band and propagation directions of the incident waves that are exploited in the seismic oceanography experiments[70,71] are comparable to those of the ballistic infrasound waves in the ocean resulting from underwater earthquakes. Thus, the seismic oceanography observations suggest that the contributions of the fine structure inhomogeneities into the scattering of ballistic waves from the earthquakes are non-negligible. Further research is needed to evaluate this mechanism of the volume scattering and its possible contribution to T-phase generation by volume scattering.

Evers *et al.*[13] reported observations of T waves in the ocean and their atmospheric counterpart, guided infrasonic waves in the atmosphere, which were generated by the same underwater earthquake. The quantitative explanation of the atmospheric observations remains elusive. We hypothesize that, akin to the abyssal T-phases, guided infrasonic waves in the atmosphere were excited by the scattering of the earthquake-generated body waves on the rough ocean surface and/or turbulence and internal gravity waves in the atmospheric boundary layer. Although quantitative analysis of the observations[13] is beyond the scope of this paper, it should be noted that Eqs. (10), (17), and (26) can be employed to assess the scattering hypothesis. A distinctive feature of the atmospheric observations by Evers *et al.*[13] is the low-frequency cutoff in the spectrum of the

earthquake-generated infrasound. The observations of the low-frequency cutoff are consistent with the predictions of Eqs. (10) and (17), as illustrated in Fig. 3 for T waves in the ocean, and provide strong support for the application of the surface scattering hypothesis to the atmospheric manifestations of underwater earthquakes.

V. CONCLUSION

The theory, which is developed in this paper from the first principles, offers a quantitative explanation of the ubiquitous observations of the efficient generation of T waves in the vicinity of the earthquake epicenter, including the earthquakes under abyssal plains with a relatively smooth seafloor. The wind waves and sea swell on the ocean surface have sufficient amplitudes for the T-phase excitation and are rich in the spatial scales needed for the Bragg scattering of ballistic body waves from the earthquake focus into the acoustic normal modes of the oceanic waveguide.

Surface scattering favors the acoustic modes, which span most of the water column, and is consistent with the T-wave observations by the receivers on the seafloor. The observations of the low-frequency cutoff in the T-wave spectra find their natural explanations in the spectral properties of the sea surface roughness. The weak correlation between the T-phase amplitude and hypocentral depth follows directly from a ray representation of the ballistic waves in a horizontally stratified fluid-solid environment. Ocean surface scattering also offers a simple explanation for the observations of the increase in the T-phase onset time with the water depth and hypocentral depth.

The contributions of the scattering by the internal gravity waves into T-wave generation are found to be negligible compared to the contributions of the surface gravity waves, among which the sea swell is expected to be the biggest contributor. The calculation of the wind-wave contribution to the conversion of the ballistic waves into T waves at the surface scattering gives the lower bound of the abyssal T-wave energy.

Our focus on the gravity wave contributions to the T-phase generation is not meant to imply that other, previously identified mechanisms are weak or unimportant. To understand the T-wave excitation, we suggest considering the sound scattering at the ocean surface in addition to the seafloor scattering and the seismic wave interaction with large bathymetric features. Presumably, depending on the local conditions, either the ocean surface scattering or the seafloor scattering may be the dominant mechanism of the abyssal T-phase generation or the two mechanisms may provide comparable contributions. The theory developed in this paper is expected to help in identifying the surface scattering contributions in the appropriate T-phase data.

Rigorous 3-D, full-wave numerical modeling (e.g., using the SPECFEM approach[12,17–19]) of the T-phase in an ocean model, which combines a large bathymetric feature with a realistic representation of the rough ocean surface, appears to be the logical next step in the investigation of the ocean surface scattering as a T-wave generation mechanism and ascertaining its significance. Further research is also needed to evaluate the significance of the sound scattering by the thermohaline fine structure and other water-column inhomogeneities as possible additional sources of the abyssal T waves and extend the theory to the atmospheric counterpart[13] of the T-phase phenomenon.

ACKNOWLEDGMENTS

This work was supported, in part, by the Office of Naval Research, Award Nos. N00014-17WX00773 and N00014-20WX01312. Helpful discussions with A. Bottero, P. Cristini, L. Evers, and R. A. Stephen are gratefully acknowledged. The author thanks the Associate Editor and three anonymous reviewers for their advice on improving the presentation.

[1]I. Tolstoy and M. Ewing, "The T-phase of shallow focus earthquakes," Bull. Seismol. Soc. Am. **40**, 25–51 (1950).
[2]C. M. Williams, R. A. Stephen, and D. K. Smith, "Hydroacoustic events located at the intersection of the Atlantis (30°N) and Kane (23°40′N) Transform Faults with the Mid-Atlantic Ridge," Geochem. Geophys. Geosyst. **7**, Q06015, https://doi.org/10.1029/2005GC001127 (2006).
[3]E. A. Okal, "The generation of T waves by earthquakes," Adv. Geophys. **49**, 1–65 (2008).
[4]J. S. Buehler and P. M. Shearer, "T phase observations in global seismogram stacks," Geophys. Res. Lett. **42**, 6607–6613, https://doi.org/10.1002/2015GL064721 (2015).
[5]J. A. Hildebrand, "Anthropogenic and natural sources of ambient noise in the ocean," Mar. Ecol. Prog. Ser. **395**, 5–20 (2009).
[6]W. S. D. Wilcock, K. M. Stafford, R. K. Andrew, and R. I. Odom, "Sounds in the ocean at 1–100 Hz," Annu. Rev. Mar. Sci. **6**, 117–140 (2014).
[7]I. F. Kadykov, *Acoustics of Underwater Earthquakes* (Nauka, Moscow, 1986) (in Russian).
[8]A. Bottero, "Full-wave numerical simulation of T-waves and of moving acoustic sources," Ph.D. thesis, Université Aix Marseille, 2018.
[9]F. K. Duennebier and R. H. Johnson, "T-phase sources and earthquake epicenters in the Pacific Basin," Technical Report, Instute of Geophysics, Hawaii University, Honolulu (1967), 100 pp.
[10]G. D'Spain, L. Berger, W. Kuperman, J. Stevens, and G. Baker, "Normal mode composition of earthquake T phases," Pure Appl. Geophys. **158**, 475–512 (2001).
[11]S. E. Freeman, G. L. D'Spain, S. D. Lynch, R. A. Stephen, K. D. Heaney, J. J. Murray, A. B. Baggeroer, P. F. Worcester, M. A. Dzieciuch, and J. A. Mercer, "Estimating the horizontal and vertical direction-of-arrival of water-borne seismic signals in the northern Philippine Sea," J. Acoust. Soc. Am. **134**(4), 3282–3298 (2013).
[12]G. Jamet, C. Guennou, L. Guillon, C. Mazoyer, and J. Y. Royer, "T-wave generation and propagation: A comparison between data and spectral element modeling," J. Acoust. Soc. Am. **134**(4), 3376–3385 (2013).
[13]L. Evers, D. Brown, K. Heaney, J. Assink, P. Smets, and M. Snellen, "Evanescent wave coupling in a geophysical system: Airborne acoustic signals from the Mw 8.1 Macquarie Ridge earthquake," Geophys. Res. Lett. **41**, 1644–1650, https://doi.org/10.1002/2013GL058801 (2014).
[14]H. Shimamura and T. Asada, "T waves from deep earthquakes generated exactly at the bottom of deep-sea trenches," Earth Planet. Sci. Lett. **27**(2), 137–142 (1975).
[15]R. Butler, "Observations of polarized seismoacoustic T waves at and beneath the seafloor in the abyssal Pacific ocean," J. Acoust. Soc. Am. **120**, 3599–3606 (2006).
[16]A. Ito, H. Sugioka, D. Suetsugu, H. Shiobara, T. Kanazawa, and Y. Fukao, "Detection of small earthquakes along the Pacific-Antarctic Ridge from T-waves recorded by abyssal ocean-bottom observatories," Mar. Geophys. Res. **33**, 229–238, https://doi.org/10.1007/s11001-012-9158-0 (2012).

[17]A. Bottero, P. Cristini, and D. Komatitsch, "Numerical simulations of *T*-wave generation and conversion at shores: Influence of slope angles and of the SOFAR channel," J. Acoust. Soc. Am. **141**, 4045 (2017).
[18]J. Lecoulant, C. Guennou, L. Guillon, and J. Y. Royer, "Three-dimensional modeling of earthquake generated acoustic waves in the ocean in simplified configurations," J. Acoust. Soc. Am. **146**, 2113–2123 (2019).
[19]A. Bottero, P. Cristini, and D. Komatitsch, "On the influence of slopes, source, seabed and water column properties on *T* waves: Generation at shore," Pure Appl. Geophys. **177**, 5695–5711 (2020).
[20]C. G. Fox, R. P. Dziak, H. Matsumoto, and A. E. Schreiner, "Potential for monitoring low-level seismicity on the Juan de Fuca Ridge using military hydrophone arrays," Mar. Technol. Soc. J. **27**, 22–30 (1994).
[21]D. K. Smith, M. Tolstoy, C. G. Fox, D. R. Bohnenstiehl, H. Matsumoto, and M. J. Fowler, "Hydroacoustic monitoring of seismicity at the slow-spreading Mid-Atlantic Ridge," Geophys. Res. Lett. **29**(11), 1518, https://doi.org/10.1029/2001GL013912 (2002).
[22]Y. Yang and D. W. Forsyth, "Improving epicentral and magnitude estimation of earthquakes from *T* phases by considering the excitation function," Bull. Seism. Soc. Am. **93**(5), 2106–2122 (2003).
[23]R. P. Dziak, S. R. Hammond, and C. G. Fox, "A 20-year hydroacoustic series of seismic and volcanic events in the northeast Pacific Ocean," Oceanography **24**(3), 280–293 (2011).
[24]H. Sugioka, Y. Fukao, and T. Hibiya, "Submarine volcanic activity, ocean-acoustic waves and internal ocean tides," Geophys. Res. Lett. **32**, L24616, https://doi.org/10.1029/2005GL024001 (2005).
[25]W. Wu, Z. Zhan, S. Peng, S. Ni, and J. Callies, "Seismic ocean thermometry," Science **369**(6510), 1510–1515 (2020).
[26]C. Wunsch, "Advance in global ocean acoustics," Science **369**(6510), 1433–1434 (2020).
[27]D. A. Walker, C. S. McCreery, and Y. Hiyoshi, "*T*-phase spectra, seismic moments, and tsunamigenesis," Bull. Seism. Soc. Am. **82**, 1275–1305 (1992).
[28]F. M. Graeber and P.-F. Piserchia, "Zones of *T*-wave excitation in the NE Indian ocean mapped using variations in backazimuth over time obtained from multi-channel correlation of IMS hydrophone triplet data," Geophys. J. Int. **158**, 239–256 (2004).
[29]N. R. Chapman and R. Marrett, "The directionality of acoustic *T*-phase signals from small magnitude submarine earthquakes," J. Acoust. Soc. Am. **119**, 3669–3675 (2006).
[30]N. R. Chapman and R. Marrett, "Reply to 'Comment on "The directionality of acoustic *T*-phase signals from small magnitude submarine earthquakes" [J. Acoust. Soc. Am. **119**, 3669–3675 (2006)],' " J. Acoust. Soc. Am. **121**, 1297–1298 (2007).
[31]D. R. Bohnenstiehl, "Comment on 'The directionality of acoustic *T*-phase signals from small magnitude submarine earthquakes' [J. Acoust. Soc. Am. **119**, 3669–3675 (2006)]," J. Acoust. Soc. Am. **121**, 1293–1296 (2007).
[32]F. K. Duennebier, "Spectral variation of the *T*-phase," Technical Report, Instute of Geophysics, Hawaii University, Honolulu (1967), 21 pp.
[33]R. H. Johnson, J. Northrop, and R. Eppley, "Sources of Pacific *T*-phases," J. Geophys. Res. **68**, 4251–4260, https://doi.org/10.1029/JZ068i014p04251 (1963).
[34]J. Talandier and E. A. Okal, "On the mechanism of conversion of seismic waves to and from *T* waves in the vicinity of island shores," Bull. Seismol. Soc. Am. **88**, 621–632 (1998).
[35]O. A. Godin, "Surface-to-volume wave conversion in shallow water with a gently sloping bottom," Acoust. Phys. **53**(6), 714–720 (2007).
[36]O. A. Godin, "Surface-to-volume wave conversion in shallow water with a corrugated bottom," Acoust. Phys. **54**(3), 346–352 (2008).
[37]R. H. Johnson, R. A. Norris, and F. K. Duennebier, "Abyssally generated *T*-phases," in *The Crust and Upper Mantle of the Pacific Area*, edited by L. Knopoff, C. L. Drake, and P. J. Hart, American Geophysical Union Geophysical Monograph No. 12 (American Geophysical Union, Washington, DC, 1968), pp. 70–78.
[38]R. E. Keenan and L. R. L. Merriam, "Arctic abyssal *T* phases: Coupling seismic energy to the ocean sound channel via under-ice scattering," J. Acoust. Soc. Am. **89**, 1128–1133 (1991).
[39]C. D. de Groot-Hedlin and J. A. Orcutt, "Synthesis of earthquake-generated *T*-waves," Geophys. Res. Lett. **26**(9), 1227–1230, https://doi.org/10.1029/1999GL900205 (1999).
[40]C. D. de Groot-Hedlin and J. A. Orcutt, "Excitation of *T*-phases by seafloor scattering," J. Acoust. Soc. Am. **109**, 1944–1954 (2001).
[41]M. Park, R. I. Odom, and D. J. Soukup, "Modal scattering: A key to understanding oceanic *T*-waves," Geophys. Res. Lett. **28**, 3401–3404, https://doi.org/10.1029/2001GL013472 (2001).
[42]R. I. Odom and D. J. Soukup, "Modal scattering and *T*-waves: Sediment amplification and source effects," J. Acoust. Soc. Am. **115**(5), 2445 (2004).
[43]W. J. Pierson and L. Moskowitz, "A proposed spectral form for fully developed wind seas based on the similarity theory of A. A. Kitaigorodskii," J. Geophys. Res. **69**, 5181–5190, https://doi.org/10.1029/JZ069i024p05181 (1964).
[44]J. H. G. M. Alves, M. L. Banner, and I. R. Young, "Revisiting the Pierson–Moskowitz asymptotic limits for fully developed wind waves," J. Phys. Oceanogr. **33**(7), 1301–1323 (2003).
[45]A. Semedo, K. Sušelj, A. Rutgersson, and A. Sterl, "A global view on the wind sea and swell climate and variability from ERA-40," J. Clim. **24**(5), 1461–1479 (2011).
[46]S. M. Flatté, R. Dashen, W. H. Munk, K. M. Watson, and F. Zachariasen, *Sound Transmission through a Fluctuating Ocean* (Cambridge University Press, Cambridge, 1979), pp. 44–61.
[47]K. L. Polzin and Y. V. Lvov, "Toward regional characterizations of the oceanic internal wavefield," Rev. Geophys. **49**(4), RG4003, https://doi.org/10.1029/2010RG000329 (2011).
[48]A. Sukhovich, J.-O. Irisson, J. Perrot, and G. Nolet, "Automatic recognition of *T* and teleseismic *P* waves by statistical analysis of their spectra: An application to continuous records of moored hydrophones," J. Geophys. Res. Solid Earth **119**, 6469–6485, https://doi.org/10.1002/2013JB010936 (2014).
[49]M. Hall, "Surface-duct propagation: An evaluation of models of the effects of surface roughness," J. Acoust. Soc. Am. **67**(3), 803–811 (1980).
[50]N. S. Gorskaya and M. A. Raevskii, "Multiple scattering of low-frequency sound waves by surface roughness," Sov. Phys. Acoust. **32**(2), 99–102 (1986).
[51]R. I. Odom, "A coupled mode examination of irregular waveguides including the continuum spectrum," Geophys. J. R. Astr. Soc. **86**(2), 425–453 (1986).
[52]R. A. Vadov, "Acoustic propagation in the subsurface sound channel," Acoust. Phys. **52**(1), 6–16 (2006).
[53]F. G. Bass and I. M. Fuks, *Wave Scattering from Statistically Rough Surfaces* (Pergamon, Oxford, 1979), Chaps. 2, 3, and 11, 525 pp.
[54]A. G. Voronovich, *Wave Scattering from Rough Surfaces* (Springer, Berlin, 1989), pp. 73–100.
[55]L. M. Brekhovskikh and O. A. Godin, *Acoustics of Layered Media. 2: Point Sources and Bounded Beams*, 2nd ed. (Springer, Berlin, 1999), pp. 16–20, 108–126, 135–144, 150–168, 263–282, and 410–414.
[56]O. A. Godin, "Calculation of amplitudes of acoustic normal modes from the reciprocity principle," J. Acoust. Soc. Am. **119**(4), 2096–2100 (2006).
[57]*Handbook of Mathematical Functions with Formulas, Graphs, and Tables*, Appl. Math. Series, Vol. 55, edited by M. Abramovitz and I. A. Stegun (Dover, New York, 1965), Sec. 9.1.
[58]O. A. Godin, "Acoustic mode reciprocity in fluid/solid systems: Implications on environmental sensitivity and horizontal refraction," in *Theoretical and Computational Acoustics*, edited by Y. C. Teng, E.-C. Shang, Y.-H. Pao, M. H. Schultz, and A. D. Pierce (World Scientific, Singapore, 1999), pp. 59–75.
[59]O. A. Godin, "On the possibility of using acoustic reverberation for remote sensing of the ocean dynamics," Acoust. Phys. **58**(1), 129–138 (2012).
[60]O. A. Godin, "Wave equation for sound in a medium with slow currents," Dokl. Akad. Nauk SSSR **293**(1), 63–67 (1987).
[61]M. S. Longuet-Higgins, "Statistical properties of wave groups in a random sea state," Phil. Trans. R. Soc. London, Ser. A: Math. Phys. Sci. **312**(1521), 219–250 (1984).
[62]L. M. Brekhovskikh and O. A. Godin, *Acoustics of Layered Media. 1: Plane and Quasi-Plane Waves*. 2nd ed. (Springer, Berlin, 1998), pp. 11–24 and 87–98.
[63]R. A. Norris and R. H. Johnson, "Submarine volcanic eruptions recently located in the Pacific by SOFAR hydrophones," J. Geophys. Res. **74**(2), 650–664, https://doi.org/10.1029/JB074i002p00650 (1969).
[64]A. E. Schreiner, C. G. Fox, and R. P. Dziak, "Spectra and magnitudes of *T*-waves from the 1993 earthquake swarm on the Juan de Fuca Ridge," Geophys. Res. Lett. **22**(2), 139–142, https://doi.org/10.1029/94GL01912 (1995).

[65]J. Hildebrand, C. G. Fox, and R. P. Dziak, "A multipath model for *T*-wave generation by seafloor earthquakes," J. Acoust. Soc. Am. **100**(4), 2639 (1996).
[66]P. D. Slack, C. G. Fox, and R. P. Dziak, "*P* wave detection thresholds, Pn velocity estimates, and T wave location uncertainty from oceanic hydrophones," J. Geophys. Res. **104**, 13061–13073, https://doi.org/10.1029/1999JB900112 (1999).
[67]O. A. Godin, "On the possible role of gravity waves in the ocean in *T*-phase excitation by earthquakes," J. Acoust. Soc. Am. **146**(4), 3068 (2019).
[68]Z. A. Der and T. W. McElfresh, "Short-period *P*-wave attenuation along various paths in North America as determined from *P*-wave spectra of the SALMON nuclear explosion," Bull. Seism. Soc. Am. **66**(5), 1609–1622 (1976).
[69]J. P. Montagner and B. L. N. Kennett, "How to reconcile body-wave and normal-mode reference Earth models," Geophys. J. Int. **125**(1), 229–248 (1996).
[70]W. T. Wood, W. S. Holbrook, M. K. Sen, and P. L. Stoffa, "Full waveform inversion of reflection seismic data for ocean temperature profiles," Geophys. Res. Lett. **35**(4), L04608, https://doi.org/10.1029/2007GL032359 (2008).
[71]R. W. Hobbs, D. Klaeschen, V. Sallarès, E. Vsemirnova, and C. Papenberg, "Effect of seismic source bandwidth on reflection sections to image water structure," Geophys. Res. Lett. **36**(24), L00D08, https://doi.org/10.1029/2007GL032359 (2009).